Title

BARYON RECOIL AND THE FRAGMENTATION REGIONS IN ULTRA-RELATIVISTIC NUCLEAR COLLISIONS

Authors

Gyulassy, M.
Csernai, L.P.

Publication Date

1986-05-01

Lawrence Berkeley Laboratory
UNIVERSITY OF CALIFORNIA

Submitted to Nuclear Physics A

BARYON RECOIL AND THE FRAGMENTATION REGIONS IN ULTRA-RELATIVISTIC NUCLEAR COLLISIONS

M. Gyulassy and L.P. Csernai

May 1986

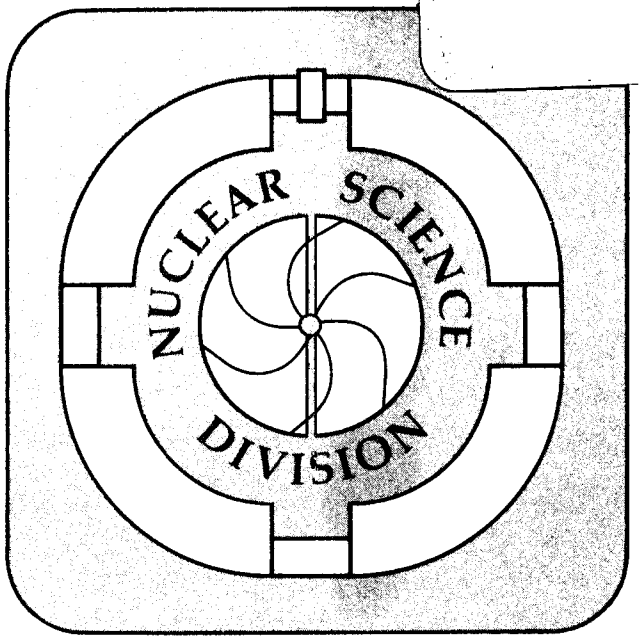

Prepared for the U.S. Department of Energy under Contract DE-AC03-76SF00098

DISCLAIMER

LBL-20610

Baryon Recoil and the Fragmentation Regions in Ultra-Relativistic Nuclear Collisions[1]

M. Gyulassy

Nuclear Science Division
Lawrence Berkeley Laboratory
University of California
Berkeley, California 94720

L.P. Csernai[2]

School of Physics and Astronomy
University of Minnesota
Minneapolis, Minnessota 55455

May 30, 1986

Abstract:

The maximum baryon and energy densities reached in the fragmentation regions of nuclear collions are estimated with a new hydrodynamical model. Unlike previous models where recoil is included as a source term for the baryon current, in our model the baryon current is strictly conserved. The parameters of the model are furthermore adjusted to take into account the large baryon rapidity shifts observed recently in $p + A \rightarrow p + X$. The implications for the production of high baryon density quark-gluons plasmas are discussed.

---

[1]Work supported by the Director, Office of High Energy and Nuclear Physics of the Department of Energy under Contract DE-AC03-76SF00098 and DE-AC02-79ER10364 and by the Minnesota Supercomputer Institute.

[2]Permanent address: Central Research Institute for Physics, Budapest, Hungary.

1. Introduction

Initial interest in the fragmentation regions of high energy nuclear collisions resulted from calculations[1] indicating that energy densities up to $\epsilon \sim 2$ GeV/fm^3 may be reached in the course of such collisions. Quantum Chromodynamic (QCD) phenomenology and lattice calculations[2] suggest that at such energy densities nuclear matter may undergo a novel transformation into a quark gluon plasma. Therefore, if indeed such energy densities could be reached, it may be possible to study the deconfinement transition in the laboratory. Subsequent analysis[3] showed that the maximum energy density increases only linearly with nuclear depth but could reach ~ 2 GeV/fm^3 at depths $\gtrsim 10$ fm. The baryon density at those depths may also reach 4-5 times nuclear saturation densities. These estimates thus indicated that the fragmentation regions in high energy collisions of heavy nuclei may shed light on the transition to high baryon density quark gluon plasmas.

However, when detailed hydrodynamic calculations[4] were performed, it was found that the maximum energy density in the fragmentation regions reached only $\sim$ 0.6 GeV/fm^3 even for U+U collisions. Other calculations[5] also suggested that the energy density in the fragmentation regions may be too small for plasma formation. Interest in the fragmentation regions therefore subsided, especially since it also became apparent[6,7] that much higher energy densities may be obtained in the low baryon density central regions. One purpose of this paper is to analyze why the detailed hydrodynamic calculations[4] led to so much smaller energy densities in the fragmentation regions. The second purpose is to update those estimates by incorporating recent nuclear stopping power results[8]-[11]. We find that the lower energy densities result from the particular way in which baryon recoil is treated in Ref.[4]. In that method the baryon current is not conserved during the initial ~ 1 fm/c of the reaction. In order to study the dependence of the results on the details of the assumed recoil mechanism, we formulate a new hydrodynamic model where the continuity equation is strictly enforced. In this model baryon recoil results from the acceleration of target partons in an effective field created in the course of the collision. The final baryon rapidity is determined by the strength of the field and the characteristic time required to neutralize the field via pair production. This model is the simplest extension of color flux tube models[12]-[17] for application to the fragmentation regions. It incorporates longitudinal growth[18] and allows us to incorporate the large A dependent baryon recoil observed recently. This model leads to to even higher energy densities ($\epsilon \sim 4$ GeV/fm^3) than the earliest estimates[1,3]. The implication of our results for the study of high baryon density plasmas via nuclear collisions is discussed at the end.

We begin by recalling the hydrodynamic equations (hereafter referred to as Model I) proposed in Ref.[4]:

$$\partial_\mu T^{\mu\nu} = \Sigma^\nu \ , \tag{1.1}$$

$$\partial_\mu n^\mu = \sigma_B \ , \tag{1.2}$$

where $T^{\mu\nu} = (\epsilon + p)u^\mu u^\nu - p g^{\mu\nu}$ is the energy momentum flux tensor in terms of the proper energy density, ϵ, pressure, p, four flow velocity, u^μ, and where the baryon

current is given by $n^\mu = \rho u^\mu$. The source terms (Σ^μ, σ_B) were constucted[19] in accordance with the inside-outside cascade picture of high energy reactions. In this picture the formation times of secondary particles are ordered such that the slower secondaries are produced before the faster ones. This ordering is a consequence of time dilation[18]. If $\tau_0 \sim 1$ fm/c is the characteristic proper time required to form a particles in its own rest frame, then the formation time or length in any other frame must grow linearly with the energy of that particle in that frame. A particle with rapidity, y, that is produced as a result of a hadronic interaction at space-time point (t_i, z_i), thus forms on the average at space-time point, $(t(y), z(y))$, given by

$$\begin{aligned} t(y) - t_i &\approx \tau_0 \cosh(y) \ , \\ z(y) - z_i &\approx \tau_0 \sinh(y) \ . \end{aligned} \tag{1.3}$$

The production of secondary particles occurs then on the average along the proper time hyperbola defined by

$$(t - t_i)^2 - (z - z_i)^2 = \tau_0^2 \ . \tag{1.4}$$

This assumed one-to-one connection between rapidity and distance made it possible[19] to relate the source terms to rapidity densities:

$$\Sigma^\mu = \sum_{z_i} \left\{ \sum_{c=\pi,B} \frac{\langle m_\perp \rangle_c}{a_\perp} \frac{dN_c}{dy} v_i^\mu 2\delta((t - z_i)^2 - (z - z_i)^2 - \tau_0^2) \right\} \ , \tag{1.5}$$

$$\sigma_B = \sum_{z_i} \left\{ \frac{1}{a_\perp} \frac{dN_B}{dy} 2\delta((t - z_i)^2 - (z - z_i)^2 - \tau_0^2) \right\} \ , \tag{1.6}$$

where $a_\perp$ is a typical transverse area (~ 3 fm^2) and $\langle m_\perp \rangle_c$ being the average transverse mass for pions or baryons. In ref.[19] it was assumed that the inclusive rapidity densities, dN_c/dy, of secondary particles are independent of projectile mass number and hence could be approximated by the empirical distribution from nucleon-nucleon collisions. The sum over z_i takes into account the contribution form all struck nucleons in the target. On the average, target nucleons are struck along the light cone at points $x_j^\mu = (z_j, z_j)$, where $z_j = j\lambda$. The inelastic mean free path of nucleons in nuclei is $\lambda = (\sigma_{in}\rho_0)^{-1} \approx 2.3$ fm. In eq.(1.5) $v_i^\mu = (x - x_i)^\mu/\tau_0$ is the four velocity of the secondaries formed at x due to an interaction at x_i as follows from (1.3). This four velocity is also the normal vector to the hadronization hyperbola $(x - x_i)^2 = \tau_0^2$ at space time point x on that hyperbola. The rapidity at which dN_c/dy is to be evaluated for source i is $y = \frac{1}{2}\ln((t+z-2z_i)/(t-z))$. Replacing the sum over z_i by an integral via $\sum_{z_i} \to \int_0^{2R} dz'/\lambda$ leads to Eqs.(4.9,4.10) of Ref.[19]. We note that the space-time region where the sources are non-vanishing is given by

$$\begin{aligned} (\tau_0^2 + z^2)^{1/2} \ \leq t \leq \ & R + (\tau_0^2 + (z - R)^2)^{1/2} \ , \\ z \ \leq t \leq \ & z + \tau_0 \ , \end{aligned} \tag{1.7}$$

where R is the thickness of the target.

The two aspects of the above hydrodynamical formulation that we call into question are the following: First, we note that Eq.(1.2) violates exact conservation of baryon number in the space time region where $\sigma_B \neq 0$. Second, the parameters, τ_0, $\langle m_\perp \rangle$, and dN_c/dy, that control the magnitude of the source terms are assumed to be independent of the projectile mass number.

Consider first the lack of exact baryon conservation. In the space time region $(t-z_0)^2-(z-z_0)^2 < \tau_0^2$, the target baryon that was initially located in the nucleus at depth z_0 is excluded from the calculation. That this could lead to a significant under estimate for the energy density can be seen as follows: Consider the contributions to the source functions from two target nucleons at depths z_0 and z_1 as illustrated in Fig. 1. Eq.(1.6) instructs us to distribute pions *and* the first recoil nucleon along the hyperbola, $(t-z_0)^2-(z-z_0)^2 = \tau_0^2$. Similarly pions and the second recoil nucleon are distributed along the hyperbola, $(t-z_1)^2-(z-z_1)^2 = \tau_0^2$. If the baryon recoil rapidity density is assumed[19] to be

$$\frac{dN_B}{dy} \approx e^{-y} \ , \tag{1.8}$$

as in pp collisions, then most of the baryon number on the first hyperbola is localized to the first few fermis from z_0 ($dN_B/dz \approx \tau_0/(2z^2)$ for $z \gg z_0$). Therefore for $z_1 - z_0$ greater than a few fermis only pions contribute appreciably to the energy deposition along the first hyperbola. For constant dN_π/dy, the energy deposition per unit length, dE_π/dz, is also a constant[3,10] because of (1.3) . Even though it may take a long time $t \approx \tau_0 \cosh(y_B)$ for the recoiling nucleon to acquire a rapidity y_B, *local* conservation of baryon current implies that the baryon current exists at all times. The dashed curve in Fig. 1 illustrates a possible recoil trajectory (see Eq.(2.3) below). At the intersection of the first hyperbola with the recoil trajectory the local energy density must include not only the contribution of the pions from the first hyperbola but also the contribution of the recoiling nucleon. The source term constructed in Eq.(1.6) neglects the contribution from the recoiling nucleon at that crossing. By the time the second nucleon is included along the second hyperbola, the energy density due to pions from the first will have decreased because of longitudinal expansion of the system[6]. We must expect then that the maximum energy density is underestimated in this model.

Consider next the second point concerning the A dependence of the source functions. The assumption[1] that those source terms are independent of A was based on the belief that the projectile fragmentation regions in p+A collisions are independent of A. Recent data has however shown[8,9,10,11] that there is in fact a significant A dependence in the projectile fragmentation region. In particular baryon recoil rapidities up to $\Delta y \sim 2.5$ units may occur for heavy nuclei. The kinematical compression[1,3] , $\rho/\rho_0 \approx \exp(\Delta y)$, alone could then increase by a factor ~ 4 using $\Delta y = 2.5$ instead of 1 as appropriate for pp collisions. The measured recoil rapidity distribution can be conveniently parameterized[10] for $n > 1$ as

$$\frac{dN_B^n}{dy} = \left(\frac{\alpha}{1-\alpha}\right)^{n-1} \frac{1}{(n-2)!} \left(e^{-y} - e^{-\alpha y} \sum_{i=2}^{n} \frac{(n-2)!}{(n-k)!} ((\alpha-1)y)^{n-k} \right) \ , \tag{1.9}$$

where $n = \nu_P \approx R_P/\lambda \sim A_P^{1/3}$ is the thickness of the projectile in terms of the number of mean free paths. Data at 100 GeV indicate that $\alpha = 3 \pm 1$. For $n = 1$ the recoil density is of course given by eq.(1.8), since this corresponds to a proton projectile.

In connection with the pion rapidity density, there is evidence[16] for an $A^{1/6}$ enhacement of the pion rapidity density in the central region in p+A collisions. In the context of color flux tube models[12]-[17], that enhancement is also coupled to an A dependent decrease of the formation time, $\tau_0 \propto A^{-1/12}$, and an A dependent increase of the transverse mass, $\langle m_\perp \rangle \propto A^{1/12}$. These effects could conspire to increase the pion source function, Σ_π^μ, by a factor $\sim A^{1/3}$ in the central region.

However, preliminary p+A data[11] indicate that the pion rapidity density in the proton fragmentation regions is insensitive to A. Unlike the leading particle (baryon) whose energy fraction, $x = \langle p_{\rm final}/p_0 \rangle$, varies from 0.5 to 0.2 as the target is varied from p to Pb, the second through the fifth fastest particles (in the kinematic region $x > 0.05$) emerge with energy fractions approximately independent of target mass. Thus, the strongest A dependence appears in the recoil baryon rapidity. In numerical estimates we will thus assume that the pion source distributions contributing to the fragmentation regions are A independent although the baryon recoil depends strongly on A.

In the next section we formulate a new hydrodynamic model obeying strictly the continuity equation, $\partial_\mu n^\mu = 0$, which allows us to evaluate the effects of A dependent recoil on the maximum attainable energy densities.

2. Formulation of the Model

Our basic idea is to treat baryon recoil as arising from acceleration of partons in an effective field, $F^{\mu\nu}$, produced in the interaction. The physical picture behind this model is based on recent chromoelectric flux tube or string models[12]-[17]. We assume that the interaction between the projectile and target nucleons leads to the formation of multiple incoherent color flux tubes. In effect the projectile and target parton clouds are "charged" up to color nonsinglet states due to multiple soft gluon exchange[13]. This leads to covariant constant color electric fields confined to flux tubes with an approximately constant a field energy per unit length or string tension, σ^*. For pp collisions we expect $\sigma^* \sim 1$ GeV/fm. For A+A collisions, a random walk in color space[12,13] may lead to a larger effective string tensions. Through pair production[14]-[17] the color fields are eventually neutralized leading in the final state to pions distributed approximately uniformly in rapidity. Of course, the string tension also acts to accelerate the partons in the target fragmentation region and to slow down the partons in the projectile fragmentation region. We assume that this is the main mechanism for baryon recoil. We will however not address the (non-Abelian) problem of how the color charged projectile and target partons accelerate coherently in the flux tube. In this paper we treat, the recoil schematically as though the baryons acquire an effective Abelian charge through soft interactions and are accelerated by the resulting fields. The phenomenological

parameters describing that field will be fixed from p+A data as stated before.

Baryon recoil in this model satisfies the simple Lorentz covariant classical equation

$$\frac{dp^\mu}{d\tau} = \frac{1}{m^*} F^{\mu\nu} p_\nu \ . \tag{2.1}$$

Transverse coordinates will be neglected throughout as we wish to retain the simplicity of the 1+1 dimensional analysis. The external field is parameterized in terms of a string tension as

$$F^{\mu\nu} = \begin{pmatrix} 0 & -\sigma^* \\ \sigma^* & 0 \end{pmatrix} . \tag{2.2}$$

This field is invariant to longitudinal boosts. For a constant string tension, the recoil rapidity from (2.1) increases linearly with proper time as $y(\tau) = \tau/\tau^*$, and the recoil baryon moves along the hyperbola

$$(z - z_0 + \tau^*)^2 - (t - z_0)^2 = (\tau^*)^2 \ . \tag{2.3}$$

The recoil time parameter is given by

$$\tau^* = m^*/\sigma^* \ , \tag{2.4}$$

where m^* is the effective mass of the recoiling baryon system.

After some proper time, τ_c, the field is neutralized through pair production, and thereafter the target baryon follows a straight line trajectory corresponding to an asymptotic recoil rapidity

$$y_r = \tau_c/\tau^* \ . \tag{2.5}$$

It is important to note that this recoil mechanism automatically builds in longitudinal growth since a target nucleon can acquire a recoil rapidity y only after a distance $z(y) - z_0 = \tau^*(\cosh(y) - 1)$. The characteristic neutralization time, τ_c, is of course not independent of τ^* since it too depends on the strength of the color electric field. An estimate of τ_c and τ^* based on nuclear stopping power data is given in section 3.1.

We implement this model for the baryon recoil in a hydrodynamic treatment by modifying Eqs.(1.1,1.2) such that

$$\partial_\mu T^{\mu\nu} = \Sigma_\pi^\nu + F^{\nu\mu} n_\mu \ , \tag{2.6}$$

$$\partial_\mu n^\mu = 0 \ , \tag{2.7}$$

where the source term Σ_π^ν is that due to pions alone in (1.6) and where $F^{\mu\nu}$ is parameterized as above. We will refer to this recoil model as Model II. We assume that the space-time region where $\Sigma_\pi^\nu \neq 0$ is the same as in Model I and given by eq.(1.7). The field is turned on as the projectile passes along the forward light cone, $t = z$. The force acting on any fluid element is assumed to be a constant until the field is neutralized. The field strength increases linearly with nuclear depth though as a result of the random charging in the wake of the projectile[13].

We furthermore adopt a simple prescription to specify the space-time region where the field is neutralized. We assume that a given fluid cell initially located

at a depth z_0 in the target accelerates under the influence of a constant force until it intersects its own neutralization hyperbola, $(t-z_0)^2-(z-z_0)^2=\tau_0^2$. We thus interpret the source hyperbolas, eq.(1.4), as color neutralization curves. In general, the location of the neutralization point can only be found numerically. However, the domain where $F^{\mu\nu}\neq 0$ in this model is contained in the region bounded by the first recoil trajectory, $z+\tau^* \geq (t^2+\tau^{*2})^{1/2}$, the last neutralization hyperbola, $t-R\leq(\tau_0^2+(z-R)^2)^{1/2}$, and $0\leq t-z\leq\tau_0$.

This model has the advantage of incorporating longitudinal growth as well as exact baryon flux conservation. The price paid is the introduction of an effective field and the necessity of modeling how it is neutralized. In principle the rate of change of four momentum flux, Σ_π^ν, due to the conversion of field energy density into secondary particles must be calculated consistently from the color neutralization equations[16,15,17]. In this paper, we will however only consider solutions of (2.6,2.7) with the above simplified model of the effective field and source term.

2.1 Equations in Comoving Variables

The hydrodynamic equations can be solved using the Lagrangian method. In that method the fluid is decomposed into many fluid cells which are followed individually as a function of time. Each cell is characterized by its flow rapidity, y, and thermodynamic quantities, ϵ, p, and ρ. We consider only the simplest type of equation of state, $p=c_0^2\epsilon$, as characterized by the speed of sound, c_0. In this case, we need only to follow the evolution of y, m^*, and ρ, where the effective mass is related to the energy density as $\epsilon=m^*\rho$. The energy momentum flux tensor can be written then as

$$T^{\mu\nu}=m^*\rho((1+c_0^2)u^\mu u^\nu-c_0^2 g^{\mu\nu}) \ . \tag{2.8}$$

With these simplifications, the hydrodynamic equations for both Model I and Model II can be written in terms local comoving variables as

$$\frac{d}{d\tau}\ln\rho = -\frac{dy}{dz'}+\frac{\sigma_B}{\rho} \ , \tag{2.9}$$

$$\frac{d}{d\tau}\ln m^* = -c_0^2\frac{dy}{dz'}+\frac{(u_\mu\Sigma^\mu)}{m^*\rho} \ , \tag{2.10}$$

$$\frac{dy}{d\tau} = \frac{1}{(1+c_0^2)}\left\{\frac{1}{\tau^*}-c_0^2\frac{d}{dz'}\ln m^*\rho-\frac{(\omega_\mu\Sigma^\mu)}{m^*\rho}\right\} \ . \tag{2.11}$$

Equation (2.9) is just the continuity equation with a baryon source term, and (2.10,2.11) are the projections of (2.6) in the directions parallel and perpendicular to u^μ. Given

$$u^\mu=(\cosh y,\sinh y) \ , \ u_\mu u^\mu=1 \ , \tag{2.12}$$

the perpendicular vector ω^μ is given by

$$\omega^\mu=(\sinh y,\cosh y) \ , \ \omega_\mu\omega^\mu=-1 \ , \ \omega_\mu u^\mu=0 \ . \tag{2.13}$$

These orthogonal vectors allow us to write

$$\frac{d}{d\tau} = u^\mu \partial_\mu \ ,$$
$$\frac{d}{dz'} = \omega^\mu \partial_\mu \ , \tag{2.14}$$

where d/dz' is the local rest frame gradient. Note that

$$\partial_\mu u^\mu = \omega^\mu \partial_\mu y = dy/dz' \ . \tag{2.15}$$

In obtaining (2.10,2.11) we have used $u_\mu F^{\mu\nu} u_\nu = 0$ and $\omega_\mu F^{\mu\nu} u_\nu = -\sigma^*$ together with the definition of τ^* in (2.4).

In this form, Model I corresponds to $\tau^* \to \infty$ and $\sigma_B \neq 0$, and Model II corresponds to $\tau^* < \infty$ and $\sigma_B = 0$. Expressed in this form, we see that whether the fluid compresses or expands depends on the sign of the flow velocity divergence, $\partial_\mu u^\mu$. This is intuitively obvious. As we shall see, the main physical difference between the two models for incorporating baryon recoil lies in the sign of that divergence. In Model I the sign is positive and hence ρ and m^* remain relatively small. In Model II the sign is negative and thereby much higher densities can be reached.

In the next section, the numerical solutions of these equations are presented. For a deeper understanding of how recoil arises in Model II, we derive in Appendix A analytic solutions in the absence of source terms. The introduction of source terms requires us to handle time-like discontinuities as derived in Appendix B. Finally, the recursion relations and numerical techniques used to solve these equations in a discretized form are derived in Appendix C.

3. Numerical Estimates

3.1 External Field Parameters

The most important recent observation from p+A studies that we want to take into account is the A dependence of the rapidity shift of the leading baryon[8,9,10,11]. The average baryon rapidity shift that follows[10] from eq.(1.9) is

$$\langle \Delta y \rangle_n = 1 + (n-1)/\alpha \quad , \tag{3.1}$$

where $n = L/\lambda$ is the average number of nucleons the projectile nucleon interacts with on traversing a slab of nuclear matter of thickness L. Empirically $\alpha = 3 \pm 1$. For impact parameter averaged p+A collisions, a fit to Glauber calculations gives

$$\nu_A \equiv \langle n \rangle_A \approx 1 + 0.57(A^{1/3} - 1) \tag{3.2}$$

for the average number of "wounded" nucleons per inelastic collision. Equations (3.1,3.2) imply for example that $\langle \Delta y \rangle_{Pb} \approx 1.9$, $\langle \Delta y \rangle_C \approx 1.2$, and $\langle \Delta y \rangle_p \approx 1.0$. For the most central collisions, for which $n \sim 6$, rapidity shifts perhaps as large as 2.5 units may occur on the average.

In our model the recoil rapidity shift is determined by the neutralization time, τ_0, and the characteristic recoil time, τ^*. We assume that the target baryon initially at depth z_0 accelerates along a recoil trajectory (C.6) until the field is neutralized. In our model, the neutralization is assumed to occur when that cell intersects the source hyperbola with its origin at (z_0, z_0). That intersection occurs in the absence of intermediate source terms at proper time, τ_c, independent of z_0 as given by

$$\frac{\tau_c}{\tau^*} = \cosh^{-1}\left(1 + \frac{\tau_0^2}{2\tau^{*2}}\right) \quad . \tag{3.3}$$

Since by eq.(2.5) this ratio is just the recoil rapidity, we see that the empirical rapidity shift (3.1) follows if we set

$$\frac{\tau_0}{\tau^*} = (2\cosh(\langle\Delta y\rangle) - 2)^{1/2} \quad . \tag{3.4}$$

The A dependence of τ_0 is correlated in color flux tube models[16,17] with the A dependence of dN_π/dy and $\langle m_\perp\rangle$. Dimensional considerations alone lead to $\langle m_\perp\rangle \propto E_0^{1/2}$ and $\tau_0 \propto E_0^{-1/2}$, where E_0 is the initial field stregth. The dimensionless rapidity density, $dN_\pi/dy \propto a_\perp E_0$ depends also on the transverse area of the flux tube, $a_\perp$. The A dependence of τ_0 can thus be fixed empirically from the measured A dependence of $\langle m_\perp\rangle$ via

$$\tau_0 \propto \langle m_\perp\rangle_A^{-1} \quad . \tag{3.5}$$

Of course longitudinal expansion can spoil this relation because the asymptotic $\langle m_\perp\rangle$ may be less than its initial value[31]. In that case (3.5) will lead to a conservative upper bound. In p+A collisions there appears to be no appreciable dependence of the transverse mass on A over the whole rapidity range[8,27]. Therefore, it is consistent to take τ_0 independent of A.

It is not known how these quantities scale with A in nuclear collisions. Possible different scenarios are discussed in Ref.[32]. We will pursue the most conservative possibility here consistent with p+A data taking τ_0 $m_\perp$, *and* dN_π/dy to be *independent* of A in the fragmentation regions where $0.03 \lesssim x \lesssim 0.3$. (The higher $x \gtrsim 0.3$ domain where dN_π/dy is known to *decrease* with A is not relevant for the problem considered here.) As noted in the introduction, recent data reported by Ledoux[11] provide the strongest evidence for the A independence of those quantities.

In our numerical estimates we therefore take the source energy density in the fragmentation regions,

$$\epsilon_\pi \approx (\langle m_\perp\rangle/\tau_0 a_\perp) dN_\pi/dy \quad , \tag{3.6}$$

to be independent of A. The dependence of τ^* on A then follows from (3.4). For Model I we employ the parameterization of Ref.[19]

$$dN_\pi/dy = 2.4(1 - 0.4e^{-y})^3 \quad . \tag{3.7}$$

For Model II we take simply $dN/dy = 2.4$ so that $\epsilon_\pi = 0.32$ GeV/fm^3.

In more optimistic scenarios[16,17,32], ϵ_π could scale as $\langle n\rangle_A$. However, we will adopt the conservative parameterization (3.4,3.6). As we shall see, this already leads to energy densities in the range of interest for quark-gluon plasma studies.

3.2 Results

The numerical solutions of eqs.(2.9,2.11), for Model I and Model II are compared in Figures 2-4. The evolution of a typical fluid cell as a function of proper time is shown in Figure 2. In this example, we follow the evolution of a cell that was initially located three mean free paths ($z_0 \approx 6.9$ fm) within the target nucleus. The energy density is shown in part (b), and the local four velocity divergence ($\partial_\mu u^\mu = dy/dz'$) as seen by that cell is shown in part (a). The solid curves (cooresponding to Model II) are labeled by thickness of the projectile nucleus in terms of the number of mean free paths, $\nu_P = 1, 3, 6$. For thicker projectiles, the field strength is greater and thus the velocity divergence is more negative. We follow the evolution of that cell until the proper time when the cell emerges from the pion source region, where $\Sigma^\mu_\pi \neq 0$. Beyond that point the final state expansion of the fluid is described by source free hydrodynamic equations. We do not solve for the subsequent expansion of the fluid since we are primarily interested in the maximum densities achieved. The dashed curve corresponds to model I with $\nu_P = 6$.

The most important difference between Model I and Model II seen in Fig. 3a is the sign of the local velocity divergence. In Model I the four divergence is always positive, whereas in our Model II the divergence is mostly *negative*. A positive divergence means that neighbooring fluid cells are receeding from one another in Model I, and hence the baryon and energy density can never build up to high values. The initial value of the velocity divergence in Model I is just $1/\tau_0$. In our model, on the other hand, the acceleration of the target cells due to the chromo-electric fields always acts to compress the fluid. This is due to the particular boundary condition whereby the field turns on along the forward light cone ($t = z$). Thus cells which were initially deeper in the target begin to accelerate at later times. As derived in Appendix A, the initial velocity divergence is just $-1/\tau^*$ in Model II. This negative velocity divergence results in the buildup of much higher energy and baryon densities. As the field neutralizes and deposits its energy into the fluid, the effective mass of the fluid cell increases. Therefore, as a function of proper time the accelerations and the magnitude of the velocity divergence decrease.

In the case $\nu_p = 6$ the four velocity divergence remains negative even at the edge of the source region ($\tau \sim 0.8$ fm/c). Therefore, the energy density will continue to increase in part (b) in this case for some time even in the source free region. In contrast, when the cell emerges at $\tau \sim 1.9$ fm/c from the source region in Model I, the energy and baryon density will immediately begin to decrease due to the large positive velocity divergence. Finally, note that in our model much higher energy densities are reached on a shorter time scale than with Model I. The kink in Fig.2 for Model II arises at the proper time when the cell enters the source region across the lower boundary (1.7), $t^2 - z^2 = \tau_0^2$. In Model I, it is assumed that there are no baryons or energy in the fluid before that source boundary.

The maximum energy and baryon density reached at the edge of the source region for cells at different initial depths is shown in Figure 3. Parts (a) and (c) show the results for our Model II, while parts (b) and (d) correspond to Model I. The dependence on the projectile thickness as measured by average number of

inelastic mean free paths, ν_P, is also indicated. The target is always taken to be six mean free paths thick ($\nu_T = 6$). The results for the special case $\nu_P = 1$ in Figures 3a,3c, and 4a are in agreement with the earlier estimates of Ref.[3]. This case corresponds to a target recoil rapidity of 1 unit in the absence of source terms.

For example, for $\nu_p = 1$ the cell initially 12 fm deep in the target is compressed at the edge of the source region in our model to $\rho \approx 4.2\ \rho_0 \approx 0.61\ \mathrm{fm}^{-3}$ with $\epsilon \approx 21.6\ \epsilon_0 \approx 2.9\ \mathrm{GeV/fm}^3$. The flow rapidity of that cell at that point is (see Figure 4a) of $y \approx 1.65$. For $\nu_P = 6$, on the other hand, that cell is compressed to significantly higher values $\rho \approx 6.7\ \rho_0$ and $\epsilon \approx 30\ \epsilon_0 \approx 4.1\ \mathrm{GeV/fm}^3$. In this case, this high baryon density fluid cell also emerges from the source region with higher rapidity $y \approx 2.2$ than in the case $\nu_P = 1$. Therefore, in our model we find that cells deep in the target can easily reach densities of interest in connection with baryon rich quark gluon plasmas.

The peak in the baryon and energy densities for shallow ($z \sim 2$ fm) cells arises because the chosen shape of the source region (see eq.(1.7)) allows those cells to accelerate in a source free region for a long time. For $z = 0$, the compression is given by the kinematic formula, $\rho/\rho_0 = \exp(y)$, derived in appendix A with flow rapiditie, y, equal to the mean flow rapidity, eq.(3.1). For shallow cells near $z \sim 2$ fm, the large rapidity mismatch between accelerated baryon fluid and the particles from the first source causes even higher compressions as in shock phenomena. In contrast, deeper cells enter the source region earlier and thus with much smaller rapidities, while the particles from the source enter with much higher rapidities from the inside-outside nature of the cascade. Therefore, the effective mass of deeper cells rises rapidly reducing their acceleration and rapidity gradient. With smaller rapidity gradients, those cells then emerge with smaller densities and rapidities than the shallow cells. Eventually, however, for very deep cells the total energy deposition from the source increases linearly as expected from Ref.[3].

We compare next the above results to those obtained using Model I. The case $\nu_P = 1$ corresponds to the source parameters used in Ref.[4]. For this case the source terms are computed using baryon and pion rapidity densities deduced from pp collisions, eqs.(1.8,3.7). We see from Figures 3b and 3d that the maximum baryon density barely reaches $2\rho_0$, and the energy density at that point is barely above 0.5 $\mathrm{GeV/fm}^3$. These densities are much lower than those that follow from Model II and confirm the pessimistic conclusions of Ref.[4] in connection with the fragmentation regions based on Model I.

Looking at curves for thicker projectiles in Fig. 3b, we find the remarkable result that the empirical stopping power of nuclei has virtually no effect on the maximum energy density obtained in Model I. The maximum baryon density only reaches $3\rho_0$ with $\nu_P = 6$. We see here explicitly how the dilution due to the large positive local velocity divergence in Model I prevents a large density buildup. A significant ν_P dependence of energy density would follow only if the pion rapidity densities in the fragmentation regions would depend on the nuclear thickness. In this model, the baryon recoil does not affect the energy density because high baryon densities are never reached.

The kinks in the curves around cell depths ~ 4 fm in Figs.3b,d arise because

cells below that point emerge from the source region (1.7) along the boundary $t = z + \tau_0$ while those originating from greater depths emerge along the source boundary $(t-R)^2 - (z-R)^2 = \tau_0^2$. Such kinks would obviously be smeared out in more realistic models.

The main qualitative effect of increasing ν_P in Model I is to shift the highest baryon density point to cells having larger recoil rapidities (compare Figure 3d with Figure 4b) . For $\nu_P = 1$ the highest baryon density is achieved for cells initially at depths $\sim$ 4 fm, which emerge with less than one unit of rapidity. For $\nu_P = 6$ the highest baryon density is achieved for cells initially at depths $\sim$ 8 fm which emerge with over 2 units of rapidity. Note that for $\nu_P = 6$ there is a long tail of moderately baryon rich matter that extends into the high rapidity region with $y \gtrsim 3$. The prescription for baryon source terms assumed in Model I together with the empirical A dependent baryon recoil densities therefore spreads the baryon flux over a wide rapidity range.

In contrast to above results, the recoil mechanism assumed in our model distributes the baryon flux over a much narrower region of rapidity. In Figure 4a, the increase of the flow rapidity with nuclear depth for $\nu_P = 1$ arises because of the increasing momentum deposition from the pion sources at greater depths. On the other hand, for $\nu_P = 6$ the baryon recoil is so large that the absorbtion of pions tends to slow down the fluid flow. The first few cells are least affected by the pion source and consequently their rapidities are close to eq.(3.1) as noted before. For $\nu_P = 6$ most cells emerge with about 2.2 units of rapidity from the source region. Thus, while the flow rapidity reflects the nuclear stopping power, the spread of rapidities is much smaller in Model II than in Model I. This is also major difference between the two models. In our model, only the *average* recoil properties can be described. This is the price we have to pay for insisting on the continuity equation, $\partial_\mu n^\mu = 0$ and incorporating recoil via an effective field. In the formulation of Model I, on the other hand, the large fluctuations of recoil rapidities can be built into the source term, σ_B, at the price of violating baryon conservation. It is of course important to observe that the flow rapidities shown in Figure 4 are those at the time of maximum compression. It is weel known that subsequent expansion of the fluid and thermal breakup will smear out the rapidity distribution of the final fragments in *any* hydrodynamical model.

We note finally the insensitivity of the above results to variations in the equation of state. In Figures 3a,3c, and 4a the dashed curve corresponds to $c_0^2 = 1/3$ and using eq.(C.14) to the change of the effective mass due the velocity divergence. The solid curves in those figures correspond to the dust equation of state. In Figures 3b,3d, and 4b the solid curves correspond to $c_0^2 = 1/3$, while the dashed curve is for the dust equation of state. The results are far more sensitive to the details of the way in which baryon recoil is implemented than to variations caused by different equations of state.

4. Discussion

In this paper we have studied two different hydrodynamic models to estimate the maximum baryon and energy densities that could be reached in the fragmentation regions of ultra-relativistic nuclear collisions. In both models we have incorporated the latest information on nuclear stopping power as deduced from $p + A \rightarrow p + X$ data. Model I, which does not conserve baryon number during the initial phase of the reaction, has the advantage that the large fluctuations of the recoil rapidities can be built into the baryon source, σ_B. Model II, which we formulated in section 2 and studied analytically in Appendix A, has the advantage that it conserves the baryon current at all times. In our model the average baryon recoil is implemented through a covariant effective field. Both models satisfy the inside-outside cascade nature of the dynamics, i.e., they take longitudinal growth into account (see further appendix A). Both models assume instantaneous local equilibration. By comparing the results of these two models, we can get an idea of the sensitivity of the results to uncertain details of the baryon recoil mechanism.

The major physical difference between these models can be seen in the sign of the four velocity divergence, $\partial_\mu u^\mu$, in Figure 2. In Model I, the source terms of both pions and baryons introduce matter into the fluid with a positive sign of that divergence. In our model, the accelerations caused by the effective field together with the forward light cone boundary condition lead to a negative velocity divergence even though color neutralization adds matter with a positive divergence to the baryonic fluid.

For the assumed average color neutralization time, $\tau_0 = 1$ fm, only Model II reaches several GeV/fm^3 and high baryon densities for cells deep in the target. It appears therefore that accelerations in addition to secondary particle production must come into play if interesting energy and baryon densities are to be generated on the average. Of course, more optimistic estimates for the neutralization time could lead to higher densities in Model I as well. However, the point is that even with conservative estimates for the neutralization time Model II densities are probably high enough to enter the deconfinement phase.

In our model these effects arise from the coupling to and neutralization of covariant fields created in the course of the collision. In conventional parton models[5], on the other hand, it is assumed that partons are simply promoted to the mass shell and propagate freely. Model I is based on a similar picture. However, partons carry color in QCD and multiple gluon exchange may leave the projectile and target parton clouds in color nonsinglet states. The rapidity mismatch of such colored parton clouds would then generate chromo-electric fields. Thus, the fields responsible for accelerations in the fragmentation regions are likely to arise naturally. What is unclear of course is how the "charges" are distributed in phase space. We have adopted a simple schematic picture in Model II, where those charges are concentrated in locally equilibrated fluid cells. A more realistic model may start with partons distributed initially according to structure functions measured in deep inelastic collisions[5] and allowing them to exchange color. This would lead to a multiple string picture where the ends of the strings are distributed in rapidity space

in a more realistic way. Secondary particles in this picture would arise then not only from the recombination of partons from the original clouds, but also from the neutralization of color fields in the course of the collsion. Such a dynamical combination of parton and string models would be interesting to study in the future. We suspect though that the resulting maximum energy and baryon density would fall between the values obtained in the two models here.

Next, we remark on fluctuations. Hydrodynamics can deal only with the average properties of the system. In rare events, there is always a finite probability to generate very high energy and baryon density "hot" spots. In this sense, any random initial condition may be generated through fluctuations. However, the evolution of such random initial conditions and the resulting signatures of quark-gluon plasma production would be extremely difficult to calculate. The great advantage of a hydrodynamical approach is that average events are well defined. For sufficiently large systems the collective, locally equilibrated behavior can be calculated through simple hydrodynamic equations. The hope with heavy ion collisions is that $Pb+Pb$, for example, is sufficiently large and the full quantum nonequilibrium theory[20] may be circumvented. However, we have seen here that even the hydrodynamic limit of the fragmentation regions will remain uncertain until we get a better understanding of the baryon recoil mechanism. This is in contrast to the central region, which, for sufficiently high energies ($E_{cm} \gtrsim 100$ GeV/A), is insensitive to that mechanism. In this regard, the upcoming CERN experiments with heavy ions up to $E_{lab} \sim$ 225 Gev/A should be useful in providing essential clues as to the correct recoil mechanism.

Finally, we note that the nonuniform compression (Figs.3a,3b) in the fragmentation regions indicates that only a fraction of the nuclear volume may reach the deconfinement phase at high baryon densities. Therefore, conventional signatures[2] of quark gluon plasma formation will be diluted by signatures from hadronic and possibly mixed phases in other parts of the nuclear volume. From Fig.4a there may not even be a clean separation in rapidity of these various contributions. On the other hand, the sandwiching of hadronic, mixed phase, and plasma phases next to each other may lead to novel collective flow or fluctuation effects since in the mixed phase the speed of sound may be significantly lower than in the hadronic or plasma phases on either side. These points should be kept in mind when analyzing the CERN data for evidence of quark-gluon plasma formation.

Acknowledgements: We are particularly grateful to R.J. Ledoux for discussions on nuclear stopping power and on his preliminary p+A data on energy fractionation[11] that motivated the choice of parameters in our model. Discussions with K. Kajantie and L. McLerran are also gratefully acknowledged.

Appendix A: Recoil in External Fields

To gain analytic insight into the way in which baryon recoil works in Model II, we solve eqs.(2.6,2.7) here in the special case $\Sigma^\mu = 0$. First we consider the simplest limit where effects due to internal pressure are neglected, i.e. $c_0 = 0$. Then we consider the perfect fluid case corresponding to a finite speed of sound. Finally, we discuss how inclusion of dissipative phenomena would affect the results.

A.1 Dust Limit

In the absence of the source term the fluid compression is due entirely to recoil in the external field. For a noninteracting gas with a "dust" equation of state $p = 0$, eq.(2.10) shows that m^* is a constant of motion, and eq.(2.11) shows that the fluid rapidity simply increases linearly with proper time:

$$y(\tau) - y(\tau_0) = (\tau - \tau_0)/\tau^* \ . \tag{A.1}$$

Since the fluid flow velocity is then $u^\mu(\tau) = (\cosh(y(\tau)), \sinh(y(\tau)))$, the trajectory of the fluid element is given by

$$\begin{aligned} t(\tau) - t_0 &= \int_{\tau_0}^{\tau} d\tau \cosh(y(\tau)) = \tau^*(\sinh(y_0 + (\tau - \tau_0)/\tau^*) - \sinh(y_0)) \\ z(\tau) - z_0 &= \int_{\tau_0}^{\tau} d\tau \sinh(y(\tau)) = \tau^*(\cosh(y_0 + (\tau - \tau_0)/\tau^*) - \cosh(y_0)) \end{aligned} \ . \tag{A.2}$$

Thus, a fluid element initially at (t_0, z_0) with velocity $u^\mu(0) = (\cosh(y_0), \sinh(y_0))$ moves in absence of a source, Σ^μ_π along the hyperbola

$$(z - z_0 + \tau^* u^0(0))^2 - (t - t_0 + \tau^* u^1(0))^2 = (\tau^*)^2 \ . \tag{A.3}$$

Note that the light cone variable, $x^- = t - z$, for the trajectory of the fluid cell is bounded between $x^-(0) \le x^- \le x^-(0) + \tau^* e^{-y_0}$. For our problem the boundary condition is that $y = 0$ on the forward light cone, i.e., $x^-(0) = 0$.

With $\sigma_B = 0$ the compression of a fluid element according eq.(2.9) obeys

$$\frac{d}{d\tau} \ln(\rho) = -\partial_\mu u^\mu \ . \tag{A.4}$$

To compute the divergence of the fluid velocity we note from (A.2) that the proper time at (t, z) is only a function of x^- because of the boundary conditions and given by

$$\tau(t, z) = \tau(x^-) = \tau_0 - \tau^* \ln\{1 - x^- e^{y_0}/\tau^*\} \ . \tag{A.5}$$

From (A.2), we see that $\partial\tau/\partial t = -\partial\tau/\partial z = \exp(y(\tau))$. Consequently, the divergence of the fluid velocity is given by

$$\partial_\mu u^\mu = \frac{\partial\tau}{\partial t}\frac{\partial u^0}{\partial\tau} + \frac{\partial\tau}{\partial z}\frac{\partial u^1}{\partial\tau} = -\frac{1}{\tau^*} \ . \tag{A.6}$$

The recoil compression from (A.4) is therefore

$$\rho(\tau) = \rho(\tau_0)\exp(y(\tau) - y(\tau_0)) \ . \tag{A.7}$$

Therefore the kinematic recoil compression formula of Ref.[1] follows from the hydrodynamic equations (2.7) in the absence of sources. Clearly, Eqs.(A.6,A.7) hold even if τ^* is allowed to depend on τ for the same boundary conditions. In that case, we need only to note that $y(\tau) - y(\tau_0) = \int_{\tau_0}^{\tau} d\tau'/\tau^*(\tau')$.

A.2 Perfect Fluid Case

The effects of internal pressure can be studied by considering a finite speed of sound in eqs.(2.10,2.11). For the boundary conditions relevant here the local gradient of the rapidity is negative, $dy/dz' < 0$, initially as seen from (A.6). Therefore, eq.(2.10) shows that m^* initially *increases*. The factor $(1+c_0^2)^{-1}$ on the r.h.s. of (2.11) shows that it is harder to accelerate the fluid due to resistence by the internal pressure. On the other hand, the local gradient of the energy density is negative initially for our boundary condition. This latter effect can at least partially compensate the first. Therefore, we expect that the main effect of including internal pressure will be to *increase* the enthalpy of the fluid.

To study quantitatively this problem we solve eqs.(2.6,2.7) in the absence of source terms for the forward light cone boundary conditions. That boundary condition implies that all field quantities depend only on the negative light cone variable, $x^- = t - z$. In terms of light cone coordinates ($x^{\pm} = t \pm z = x_{\mp}$):

$$n^{\pm} = n_{\mp} = \rho(u^0 \pm u^1) \ = \ \rho\exp(\pm y) \tag{A.8}$$

$$\begin{pmatrix} T^{++} & T^{+-} \\ T^{-+} & T^{--} \end{pmatrix} = \begin{pmatrix} h_+ e^{2y} & h_- \\ h_- & h_+ e^{-2y} \end{pmatrix} \tag{A.9}$$

$$\begin{pmatrix} F^{++} & F^{+-} \\ F^{-+} & F^{--} \end{pmatrix} = \begin{pmatrix} 0 & 2\sigma^* \\ -2\sigma^* & 0 \end{pmatrix} \ , \tag{A.10}$$

where the thermodynamic functions, $h_{\pm}$, in (A.9) are related to the energy density, ϵ, and pressure, p, via

$$h_{\pm} = \epsilon \pm p \ . \tag{A.11}$$

With the forward light cone boundary condition corresponding to

$$n^{\pm}(x^- \leq 0) \ = \ \rho_0 \tag{A.12}$$

$$h_{\pm}(x^- \leq 0) \ = \ \epsilon_0 \tag{A.13}$$

$$y(x^- \leq 0) \ = \ 0 \tag{A.14}$$

$$\sigma^*(x^- \leq 0) \ = \ 0 \ , \tag{A.15}$$

all fluid variables depend only on x^- in the absence of source terms ($\Sigma^{\mu} = 0$). We assume that $p(x^- \leq 0) = 0$ according to (A.13).

The continuity equation reduces in this case to

$$\partial_\mu n^\mu = \partial_- n^- = \partial_-(\rho e^{-y}) = 0 \ , \tag{A.16}$$

with $\partial_- = d/dx^-$. This means that n^- is a constant of motion with a value as determined from (A.12,A.14) given by

$$n^- = n_+ = \rho(x^-)e^{-y(x^-)} = \rho_0 \ . \tag{A.17}$$

We thus see that the kinematical compression formula (A.7) is completely general for these boundary conditions.

Noting next that $\partial_\mu T^{\mu\nu} = \partial_- T^{-\nu}$ and $F^{\nu\mu}n_\mu = \frac{1}{2}(F^{\nu+}n_+ + F^{\nu-}n_-)$, the equations of motion reduce to

$$\partial_- T^{--} = \partial_-(h_+ e^{-2y}) = -\sigma^* n^- = -\sigma^* \rho_0 \tag{A.18}$$

$$\partial_- T^{-+} = \partial_- h_- = \sigma^* \rho_0 e^{2y} \ . \tag{A.19}$$

The solution of (A.18) for a constant string tension σ^* is simply

$$h_+(x^-) = \epsilon_0(1 - x^-/\tau^*)e^{2y(x^-)} \ , \tag{A.20}$$

where the critical recoil time scale is given by

$$\tau^* = \epsilon_0/(\sigma^* \rho_0) \ . \tag{A.21}$$

Up to this point we have not had to specify the equation of state for the fluid. However, to solve (A.19) we must relate $h_- = \epsilon - p$ to $h_+ = \epsilon + p$. We consider here the simplest equation of state characterized by a speed of sound, c_0,

$$p = c_0^2(\epsilon - \epsilon_0) \ . \tag{A.22}$$

In this case (A.19) reduces to

$$\begin{aligned} \partial_- h_- &= \frac{(1-c_0^2)}{(1+c_0^2)} \partial_- h_+ \\ &= \frac{(1-c_0^2)}{(1+c_0^2)} \epsilon_0 e^{2y} \left\{ 2(1 - x^-/\tau^*)\partial_- y - 1/\tau^* \right\} \\ &= \frac{\epsilon_0}{\tau^*} e^{2y} \ . \end{aligned} \tag{A.23}$$

The fluid flow rapidity is thus given by

$$y(x^-) = -\frac{1}{1-c_0^2} \ln(1 - x^-/\tau^*) \ . \tag{A.24}$$

Substituting (A.24) into (A.17,A.20) leads finally to

$$\rho(x^-) = \rho_0(1 - x^-/\tau^*)^{-\frac{1}{1-c_0^2}} \tag{A.25}$$

$$h_+(x^-) = \epsilon_0(1 - x^-/\tau^*)^{-\frac{1+c_0^2}{1-c_0^2}} \ . \tag{A.26}$$

The fluid flow is thus bounded between $0 \leq x^- \leq \tau^*$. As x^- approaches τ^* the fluid rapidity, density, and enthalpy all diverge.

It is also useful to express these flow characteristics as a function of proper time. For a fluid element at x^- and any value of x^+, the proper time is given by

$$\tau(x^-) = \int_0^{x^-} dx\, e^{y(x)} = \tau^* \frac{(1-c_0^2)}{c_0^2} \left[\left(\frac{1}{1 - x^-/\tau^*} \right)^{\frac{c_0^2}{1-c_0^2}} - 1 \right] . \qquad \text{(A.27)}$$

The flow characteristics at proper time, τ, are thus given by

$$y(\tau) = \frac{1}{c_0^2} \ln \left(1 + \frac{c_0^2}{1-c_0^2} \frac{\tau}{\tau^*} \right) \qquad \text{(A.28)}$$

$$\rho(\tau) = \rho_0 \left(1 + \frac{c_0^2}{1-c_0^2} \frac{\tau}{\tau^*} \right)^{1/c_0^2} \qquad \text{(A.29)}$$

$$h_+(\tau) = \epsilon_0 \left(1 + \frac{c_0^2}{1-c_0^2} \frac{\tau}{\tau^*} \right)^{1+1/c_0^2} . \qquad \text{(A.30)}$$

For $c_0^2 \to 0$, (A.28) reduces to (2.5) and both ρ and h_+ increase exponentially with proper time.

The trajectory of a fluid element which was initially at rest at position ($x^- = 0, x^+ = x_0$) at proper time $\tau = 0$ is given by

$$x^-(\tau) = \int_0^\tau d\tau' e^{-y(\tau')} = \tau^* \left[1 - \left(1 + \frac{c_0^2}{1-c_0^2} \frac{\tau}{\tau^*} \right)^{1-\frac{1}{c_0^2}} \right] \qquad \text{(A.31)}$$

$$x^+(\tau) = x_0 + \int_0^\tau d\tau' e^{y(\tau')} = x_0 + \tau^* \frac{(1-c_0^2)}{(1+c_0^2)} \left[\left(1 + \frac{c_0^2}{1-c_0^2} \frac{\tau}{\tau^*} \right)^{1+\frac{1}{c_0^2}} - 1 \right] \qquad \text{(A.32)}$$

Of course, in the dust limit, $c_0 = 0$, (A.31,A.32) reduce to (A.2).

Figure 5 shows the proper time development of the recoil characteristics for different equation of states. The solid curves correspond to the dust limit ($c_0 = 0$). The dashed curves correspond to $c_0^2 = 1/6, 1/3$. The solutions depend on the ratio of the proper time to the characteristic recoil time τ^* (A.21) that measures the strength of the external field. We are interested in these solutions up to the characteristic neutalization time, τ_c, of the external field. Since the empirical[8,9,10] baryon recoil rapidity is less than three units for the heaviest nuclei, from Fig.5a we see that only times up to $\tau/\tau^* \lesssim 3$ are relevant.

In that proper time range, the solutions display a number of interesting features. First, the pressure gradients actually help in compressing the fluid. Thus, even though internal pressure eventually inhibits the compression at later times ($\tau/\tau^* \gtrsim 3$) as expected intuitively, at the early times of interest, the pressure gradients $\partial p/\partial z > 0$ induced by the external field overcompensate initially the increased resistance of the fluid to compression. Second, the overall sensitivity of the recoil rapidity and compression to the equation of state is small. On the other hand, the

enthalpy could increase by a factor of two in the interesting range of times. Thus, the main effect of including the internal pressure is to heat rather than to compress the fluid in this case. The most important qualitative conclusion we draw from Fig.5 is that the use of the dust equation of state gives a conservative lower bound on the enthalpy resulting from recoil.

A.3 Dissipative Effects

The results of the previous section apply only to perfect fluids. If the mean free paths, λ, are not small compared to the scale of the gradients of fluid properties, then dissipative phenomena[21,22,23] must be considered. To first order in the gradients (the Navier-Stokes approximation), the energy-momentum tensor and the baryon current in eqs.(2.6,2.7) are given by

$$T^{\mu\nu} = (h_+ u^\mu u^\nu - p g^{\mu\nu}) + \tau^{\mu\nu} \ , \tag{A.33}$$

$$n^\mu = \rho u^\mu + \nu^\mu \ , \tag{A.34}$$

where for the forward light cone boundary conditions (A.15) the correction terms can be expressed as

$$\begin{pmatrix} \tau^{++} & \tau^{+-} \\ \tau^{-+} & \tau^{--} \end{pmatrix} = (\frac{4}{3}\eta + \varsigma) \begin{pmatrix} -e^{2y} & 1 \\ 1 & -e^{-2y} \end{pmatrix} \partial_- u^- \ , \tag{A.35}$$

$$\begin{pmatrix} \nu^+ \\ \nu^- \end{pmatrix} = \kappa \left(\frac{\rho T}{h_+}\right)^2 \begin{pmatrix} 1 \\ -e^{-2y} \end{pmatrix} \partial_- \left(\frac{\mu_B}{T}\right) \ . \tag{A.36}$$

The three transport coefficients, η, ς, κ, corresponding to shear viscocity, bulk viscocity, and thermal conductivity control the magnitude of these corrections. They are all proportional to the transport mean free path, λ. Kinetic theory estimates for them using QCD phenomenology were given in Ref.[21,22,23]. In (A.36), μ_B is the baryon chemical potential and T is the temperature. The equation of state specifies the enthalpy, h_+, as a function of μ_B and T.

We note that unlike for the case of low baryon density plasmas generated in the central rapidity regions, thermal conductivity can play an important role in the high baryon density fragmentation regions. The way in which thermal conductivity enters depends, however, on the definition of the fluid local rest frame. The Landau local rest frame is that in which the energy three flux, T^{01}, vanishes. The Eckart local rest frame is that in which the baryon three current , n_i, vanishes. In general, it is not possible to insure that both fluxes vanish. Because of the artificial singularity of heat conduction phenomena with the Eckart definition for $\mu_B \ll T$, it is convenient to work with the Landau one[22]. Eqs.(A.33-A.36) correspond to the Landau definition since $T^{01} = (T^{++} - T^{--})/4 = 0$ in the frame where $y = 0$. Heat conduction in this case leads to a finite baryon three current, $n^1 = \kappa(\rho T/h_+)^2 \partial_-(\mu_B/T)$, in the fluid rest frame. For a quark-gluon plasma with N_c colors and N_f flavors, Eq.(2.15) of Ref.[22] gives

$$\kappa = \begin{cases} \frac{N_c N_f}{81} \lambda T \mu_B^2 & \text{for } \mu_B \gg 3\pi T \\ \frac{16 K^2}{N_c N_f} \lambda T^5/\mu_B^2 & \text{for } \mu_B \ll T \end{cases} \ , \tag{A.37}$$

where $K = (N_c^2 - 1 + 7N_cN_f/4)\pi^2/15$ is the Stephan-Boltzmann constant. Remarkably, even though the form of κ is so different in the two extreme limits, the correction to the baryon current in both cases is given by

$$\nu^- = -\frac{N_cN_f}{81}\lambda T^3 e^{-2y}\partial_-(\mu_B/T) \ . \tag{A.38}$$

In both cases the contributions to κ from quarks and antiquarks dominate the contribution from gluons. Since (A.38) works in both limits, it may be adequate for most purposes even in the interesting $\mu_B \sim 3T$ region. Of course, the most difficult problem is estimating the transport mean free path, $\lambda(\mu, T)$. In Ref.[22] simple QCD phenomenological estimates indicated that for the range of temperatures and densities of interest, nonperturbative anti-screening and color magnetic screening effects would have to be large in order for the transport mean free paths to be significantly less than 1 fm.

The continuity equation in our case still insures that n^- is a constant of motion:

$$n^- = \rho e^{-y} + \nu^- = \rho_0 \ . \tag{A.39}$$

Furthermore, since $\nu^+ = -\nu^- e^{2y}$,

$$n^+ = \rho e^{y} + \nu^+ = (\rho_0 - 2\nu^-)e^{2y} \ . \tag{A.40}$$

Equations (A.18,A.19) are thus replaced by

$$\partial_-(e^{-2y}[h_+ - \chi\partial_- u^-]) = -\frac{\epsilon_0}{\tau^*} \ , \tag{A.41}$$

$$\partial_- h_- = \frac{\epsilon_0}{\tau^*}(1 - \frac{2\nu^-}{\rho_0})e^{2y} \ , \tag{A.42}$$

where $\chi = \frac{4}{3}\eta + \zeta$. Unfortunately, all three equations (A.39,A.41,A.42) for the three unknonws, $y(x^-), \mu_B(x^-), T(x^-)$ are now coupled and can be solved only numerically.

We can however get a rough idea of the nature of those solutions if the viscocity coefficients are approximated as in elementary kinetic theory by

$$\chi \approx \frac{1}{3}\lambda h_+ \ . \tag{A.43}$$

In that case, (A.41) yields

$$h_+ = \epsilon_0 e^{2y}\frac{(1 - x^-/\tau^*)}{(1 - \frac{1}{3}\lambda\partial_- u^-)} \ . \tag{A.44}$$

We can estimate to lowest order in λ the gradient of u^- from (A.24) to be

$$\partial_- u^- \approx -\frac{(1 - x^-/\tau^*)^{c_0^2/(1-c_0^2)}}{(1 - c_0^2)\tau^*} \ . \tag{A.45}$$

Inserting this estimate into (A.44) shows that viscocity tends to reduce the enthalpy by a factor $\sim 1/(1+\lambda/3\tau^*)$. (Note that we are assuming that since y and ρ in Fig.5 are not sensitive to the equation of state for times of interest, e^{2y} can also be approximated by its perfect fluid value.) Even though the magnitude of the transport mean free paths in a quark gluon plasma are very uncertain, the dimensionless ratio $\lambda/3\tau^*$ is likely to be on the order of unity. Thus, the enthalpy could be about a factor of two lower than the ideal fluid value. From Fig.5 we thus see that the main effect of dissipative phenomena would be the lowering of the enthalpy to the dust equation of state value. Since the recoil rapidity and compression are insensitive to the effects of pressure, dissipative phenomena would not be expected to play an important role for these quantities. Just as in Refs.[7,22] we expect the solutions including dissipative effects to fall in the region between the $c_0^2 = 0$ and $1/3$ curves in Fig.5. Furthermore, any sharp peaks as in Fig.3a would be smeared out by dissipative effects, especially since they occur only one mean free path within the target.

Appendix B: Pion Source Terms

B.1 Time-like Discontinuity Equations

In Appendix A we studied the pure recoil case without pion source terms in (2.6). That recoil was due entirely to the acceleration in an external field $F^{\mu\nu}$ which we parameterize by an effective string tension in (2.2). The acceleration ceases in this model when the field is neutralized by pair production. However, the energy stored in the field must also be accounted for. Physically, the neutralization process is the mechanism by which the energy stored in the field is converted into energy in the matter fields. The source term, Σ_π^ν, is included in (1.5) to take into account this additional source of energy and momentum in the matter fields. Unfortunately, it is not yet known how to treat the effective external field and its neutralization self consistently. Preliminary work in that direction can be found in Refs.[15,13,17,14,12].

To gain at least a qualitative understanding of the effect of such source terms, we proceed here in the spirit of Ref.[4,19,25] and treat the neutralization schematically via Eq.(1.5). We assume that each struck target nucleon contributes an independent string that neutralizes along a proper time curve characterized by a proper time, τ_0. We thus parameterize the i^{th} source function as

$$\Sigma_i^\mu(x) = \epsilon_\pi v_i^\mu(x)\delta(v_i^\mu(x)v_{i\mu}(x) - 1)/\tau_0 \ , \tag{B.1}$$

with $v_i^\mu(x) = (x - x_i)^\mu/\tau_0$ as in (1.6). The proper energy density, ϵ_π, of the matter produced along the neutralization hyperbola must be proportional to the effective string tension, σ^*, since both are proportional to the initial field energy density.

The interpretation of Σ_i^μ is made easier by noting that if $T^{\mu\nu}$ were zero below the hyperbola defined by $v_i^\mu(x)v_{i\mu}(x) = 1$, then integrating $\partial_\mu T^{\mu\nu} = \Sigma_i^\nu$ across the hyperbola would give $T^{\mu\nu} = \epsilon_\pi v_i^\mu(x)v_i^\nu(x)$. Thus we can interpret Σ_i^μ as the source of particles with zero baryon charge, energy density ϵ_π, zero pressure, and flow velocity

v_i^μ resulting from the partial neutralization of the field along the i^{th} neutralization hyperbola.

The sudden deposition of energy and momentum into the recoiling fluid leads of course to a discontinuity of the flow pattern along each of the source hyperbolas. What is unusual about this discontinuity surface is that its normal vector is time-like. Recall that $v_i^\mu(x)$ is the normal vector to the i^{th} hyperbola at position x with the property

$$v_i^\mu v_{\mu i} = 1 \ . \tag{B.2}$$

Familiar shock and detonation discontinuities, on the other hand, have space-like normal vectors[24,28] with $v^\mu v_\mu = -1$. (Note that we use the sign convention of [28] which is opposite of Ref.[24]).

Time-like discontinuities can be treated in a manner very similar to space-like discontinuities as shown in Ref.[26]. For the case of discontinuities along proper time hyperbolas as in Eq.(B.1), this generalization is particularly transparent. Because time-like discontinuities are unfamiliar, we derive in detail below the relevant discontinuity equations.

In order to calculate the i^{th} discontinuity, it is convenient to change variables to

$$\tau = ((t-t_i)^2 - (z-z_i)^2)^{1/2} \ , \tag{B.3}$$

$$\eta = \frac{1}{2}\ln((t+z-t_i-z_i)/(t-z-t_i+z_i)) \ , \tag{B.4}$$

where (t_i, z_i) is the location of the i^{th} interaction in the target. The volume element is then given by $d^4x = \tau d\tau d\eta d^2x_\perp$. In these coordinates the normal vector at point $x^\mu = x_i^\mu + \tau_0(\cosh\eta, \sinh\eta)$ along the i^{th} hyperbola is given by

$$v_i^\mu = \frac{\partial\tau}{\partial x_\mu} = (\cosh\eta, \sinh\eta) \ , \tag{B.5}$$

and the tangent vector to the discontinuity is given by

$$w_i^\mu = -\tau\frac{\partial\eta}{\partial x_\mu} = (\sinh\eta, \cosh\eta) \ . \tag{B.6}$$

Note that $w_i^\mu w_{\mu i} = -1$ and $v_i^\mu w_{\mu i} = 0$. The divergence operator is then given by

$$\partial^\mu = v_i^\mu\frac{\partial}{\partial\tau} + \frac{w_i^\mu}{\tau}\frac{\partial}{\partial\eta} \ . \tag{B.7}$$

We suppress transverse coordinates throughout.

The first discontinuity equation is trivial. The baryon continuity equation (2.7) of course implies that all components of the baryon current are continuous. In particular the component of the baryon current along the normal to the discontinuity is continuous. Denoting that component across the i^{th} hyperbola by

$$J_i \equiv \rho u_\mu v_i^\mu = \rho\cosh(y-\eta) \ , \tag{B.8}$$

we have

$$[J_i] = 0 \ , \tag{B.9}$$

where $[f(\tau)] = f(\tau + 0^+) - f(\tau - 0^+)$ denotes the discontinuity across the source singularity, and $y(\tau, \eta)$ is the fluid rapidity.

The second set of discontinuity equations follow upon integrating the equations of motion (2.6) over a 4-volume element enclosing an infinitesmal section of the 3-hypersurface defined by the i^{th} neutralization hyperbola. Consider a 4-volume $\delta V = \tau_0 \Delta\tau \Delta\eta a_\perp$. The field contribution, $\int_{\delta V} d^4x F^{\mu\nu} n_\mu$, is second order, $O(\Delta\tau\Delta\eta)$, and thus can be neglected in the limit $\Delta\tau \to 0$ and $\Delta\eta \to 0$. Since the i^{th} source can be written

$$\Sigma_i^\mu = \epsilon_\pi v_i^\mu \delta(\tau - \tau_0) \ , \tag{B.10}$$

the integral over the source is simply

$$\int_{\delta V} d^4x \Sigma_i^\mu = a_\perp \tau_0 \Delta\eta \epsilon_\pi v_i^\mu \ . \tag{B.11}$$

With (B.7) we see next that to first order in infinitesmals $\Delta\tau, \Delta\eta$

$$\int_{\delta V} d^4x \partial_\mu T^{\mu\nu} = a_\perp \tau_0 \Delta\eta [T^{\mu\nu} v_{\mu i}] \ . \tag{B.12}$$

Equating (B.11) with (B.12) gives therefore in the $\Delta\tau \to 0$ and $\Delta\eta \to 0$ limit

$$[T^{\mu\nu} v_{\mu i}] = \epsilon_\pi v_i^\nu \ . \tag{B.13}$$

Projecting this vector discontinuity equation into v and w directions gives the following two discontinuity equations:

$$[h \cosh^2(y - \eta) - p] \ = \ \epsilon_\pi \ , \tag{B.14}$$

$$[h \sinh(y - \eta) \cosh(y - \eta)] \ = \ 0 \ , \tag{B.15}$$

where $h \equiv h_+ = \epsilon + p$ is the enthalpy. Equations (B.9,B.14,B.15) determine the density, enthalpy, and flow rapidity after the singularity as a function of those quantities before the singularity and as a function of the source energy density, ϵ_π.

To solve those equations we note first from (B.9) that

$$\cosh(y - \eta) = J_i/\rho \ . \tag{B.16}$$

Substituting into (B.14) gives then[25,26]

$$J_i^2 = (\epsilon_\pi + [p])/[X] \ , \tag{B.17}$$

in terms of the discontinuity of the generalized specific volume[29,30]

$$X = h/\rho^2 \ . \tag{B.18}$$

Next squaring (B.15) and using (B.16) again, we find another expression for J_i^2 given by

$$J_i^2 = [hX]/[X^2] \ . \tag{B.19}$$

Finally, combining (B.17) and (B.19) give rise to the Taub adiabat for this problem

$$([p] + \epsilon_\pi)[X^2]/[X] = [hX] \ . \tag{B.20}$$

For a given equation of state, (B.20) defines a curve on the (p, X) plane on which the solution lies. For a given incident baryon current, J_i, (B.17) defines a second curve. The solution is at the intersections of those two curves. The difference between space-like and time-like discontinuities[26] appears in eq.(B.17) while eq.(B.20) holds in both cases.

For the dust equation of state ($h = m\rho$) the discontinuity equations can be easily solved to give

$$\begin{aligned} m_2^2 &= m_1^2 + 2m_1\epsilon_\pi/\rho_1 + (\epsilon_\pi/J_i)^2 \ , & \text{(B.21)} \\ \rho_2 &= m_2/(m_1/\rho_1 + \epsilon_\pi/J_i^2) \ , & \text{(B.22)} \\ u_2^\mu &= (m_1/m_2)u_1^\mu + (\epsilon_\pi/m_2 J_i)v_i^\mu \ , & \text{(B.23)} \end{aligned}$$

where $J_i = \rho_1 \cosh(y_1 - \eta)$ and subscripts 1 and 2 refer to quantities before and after the singularity at the point $x^\mu = x_i^\mu + \tau_0(\cosh\eta, \sinh\eta)$ along the i^{th} hyperbola.

In order to compare the results to those obtained earlier solving Eqs.(1.1,1.2), we also quote the discontinuity equations for the case when (2.7) is replaced by (1.2). With a baryon source, σ_i, placed on the i^{th} hyperbola, eq.(B.9) is replaced by

$$[\rho \cosh(y - \eta)] = \sigma_i \ . \tag{B.24}$$

The solution of (B.24,B.14,B.15) for the dust equation of state is

$$\begin{aligned} m_2^2 &= (J_i/(J_i + \sigma_i))^2\{m_1^2 + 2m_1\epsilon_i/\rho_1 + (\epsilon_i/J_i)^2\} \ , & \text{(B.25)} \\ \rho_2 &= ((J_i + \sigma_i)/J_i)^2\{m_2/(m_1/\rho_1 + \epsilon_i/J_i^2)\} \ , & \text{(B.26)} \\ u_2^\mu &= (J_i/(J_i + \sigma_i))\{(m_1/m_2)u_1^\mu + (\epsilon_i/m_2 J_i)v_i^\mu\} \ . & \text{(B.27)} \end{aligned}$$

These equations of course reduce to (B.21-B.23) in the limit $\sigma_i \to 0$. In the case $\sigma_i \neq 0$, ϵ_i includes a contribution from baryons as well as pions as in eq.(1.5).

B.2 Propagation Between Discontinuities

Between discontinuities the fluid evolves according to eqs.(2.9-2.11) with $\Sigma^\mu = 0$. Again we restrict ourselves to the simplest case corresponding to the dust equation of state for which m^* remains a constant between discontinuities. In this case eq.(2.11) leads to eqs.(A.1-A.3). Consider a fluid cell at (t_0, z_0) with rapidity y_0 at proper time τ_0. Suppose that the local rest frame rapidity gradient, $dy/dz' \equiv y'$

is known at τ_0. A neighboring cell located at an infinitesmal distance, δ, in that frame has then a rapidity $y'\delta$ relative to the first cell. Because of the rapidity gradient, these adjacent fluid cells move apart or together depending on the sign of y'. Consequently, the local density will decrease or increase respectively as (2.9) instructs. We can solve for the (de)compression as a function of proper time by following the evolution of these two cells according to eq.(A.3). It is of course most convenient to work in the frame where the first cell is at rest at $t = 0$, $z = 0$, and the second cell has $y = y'\delta$ at $t = 0$, $z = \delta$. In that frame the cells move along the hyperbolas

$$z(t) = (t^2 + \tau^{*2})^{1/2} - \tau^* \ , \tag{B.28}$$

$$z_\delta(t) = z(t) + \delta(1 + v(t)\tau^* y') + O(\delta^2) \ , \tag{B.29}$$

where the velocity of the first cell is given by

$$v(t) = t/(t^2 + \tau^{*2})^{1/2} \ . \tag{B.30}$$

Note that in this frame $v(0) = 0$ and thus $z_\delta(0) = \delta$.

Since at time, t_1, the first cell has velocity, $v_1 = v(t_1)$, the local rest frame z' axis is given by

$$z = z(t_1) + (t - t_1)/v_1 \ . \tag{B.31}$$

When the first cell is located at $(t_1, z(t_1))$ the location of the second cell at the *same* local time is given by $(t_2, z_\delta(t_2))$, with t_2 determined from

$$z_\delta(t_2) = z(t_1) + (t_2 - t_1)/v_1 \ . \tag{B.32}$$

The solution of (B.32) to first order in δ is simply

$$t_2 = t_1 + \delta(1 + v_1\tau^* y')\gamma_1^2 v_1 \ , \tag{B.33}$$

with $\gamma_1 = (1 - v_1^2)^{-1/2}$.

The local rest frame separation of those cells when the first cell is located at $(t_1, z(t_1))$ is thus given by

$$\Delta z' = (z_\delta(t_2) - z(t_1))/\gamma_1 = \delta(1 + v_1\tau^* y')\gamma_1 \ . \tag{B.34}$$

Recalling that $(\gamma_1, \gamma_1 v_1) = (\cosh(y(t_1)), \sinh(y(t_1))$ in terms of the rapidity, $y(t)$, of the first cell, and recalling eq.(A.1) we obtain finally the following general expression for the separation of the fluid cells as a function of proper time

$$\Delta z'(\tau) = \delta(\cosh(\tau/\tau^*) + y'\tau^* \sinh(\tau/\tau^*)) \ , \tag{B.35}$$

where $\Delta z'(0) = \delta$ and y' is the initial local rapidity gradient.

Equation (B.35) allows us to compute the (de)compression factor for propagating between discontinuities:

$$\frac{\rho(\tau)}{\rho(\tau_0)} = (\cosh(\Delta\tau/\tau^*) + y'(\tau_0)\tau^* \sinh(\Delta\tau/\tau^*))^{-1} \ , \tag{B.36}$$

where $\Delta\tau = \tau - \tau_0$. It is easy to verify that the forward light cone boundary conditions are equivalent to $y'(0)\tau^* = -1$, and thus (B.36) reduces to the simple kinematic recoil formula (A.7) in that case. Note also that in the absence of an external field, $\tau^* \to \infty$, and eq.(B.36) reduces to the intuitive geometrical relation

$$\frac{\rho(\tau)}{\rho(\tau_0)} = (1 + y'\Delta\tau)^{-1} \ . \tag{B.37}$$

Form (B.36,B.37) it is clear that compression will occur only if $y' < 0$. However, if $-y'$ is too large, then the propagation between discontinuities may lead to a singularity. In that case shocks may develop and the methods used here would have to be modified. For our applications, though, shocks are not generated.

We now have all the equations necessary to compute the recoil trajectories including the pion source terms. The recursion formulas used to evolve the fluid cells between the pion source hyperbolas via eq.(B.36) and to jump across the sources via eqs.(B.21 -B.23) are presented in Appendix C.

Appendix C: Recursion Formulas for Recoil Trajectories

The numerical results were obtained by evolving fluid cells according to the discontinuity and propagation formulas derived in Appendix B. We approximated the source function, Σ^μ, by a series of hyperbolas spaced λ/N_s apart with N_s ranging between 10 and 100 to test for convergence. The target nucleus was divided into cells of dimensions, λ/N_c, with with N_c varying between $10 - 30N_s$. The figures for Model II show results for $N_s = 50$ and $N_c = 500$. For Model I we used a coarser grid with $N_s = N_c = 10$ since convergence is more rapid in that model. We demanded numerical convergence to only a few percent accuracy. Input parameters were taken as $m_N = 0.938$ MeV, $\rho_0 = 0.145$ fm^{-3}, $\tau_0 = 1$ fm, $a_\perp = 3$ fm^2, $\lambda = 2.3$ fm. The A dependent field strength, σ^*, is fixed according to eq.(3.4) in section 3.1. For $\nu_P = 6$ for example, $\sigma^* = 3.311$ GeV/fm.

The n^{th} source leads to a time-like discontinuity along the hyperbola

$$(t - n\lambda/N_s)^2 - (z - n\lambda/N_s)^2 = \tau_0^2 \ . \tag{C.1}$$

The m^{th} recoiling fluid element, initially at depth $m\lambda/N_c$, begins to accelerate at time $m\lambda/N_c$ and moves along the recoil hyperbola

$$(z - m\lambda/N_c + \tau^*_{m0})^2 - (t - m\lambda/N_c)^2 = (\tau^*_{m0})^2 \ , \tag{C.2}$$

where $\tau^*_{m0} = m_N/\sigma^*$ is the initial acceleration time constant. Because m^* changes so will that acceleration contant after the first discontinuity. That fluid element encounters the first source at point (t_{m1}, z_{m1}) as obtained by solving for the relevant intersection of eqs.(C.1,C.2) with $n = 1$. Just before that singularity the flow rapidity and baryon density are given by Eqs.(A.24, A.25) with $x^- = t_{m1} - z_{m1}$. We denote these quantities by y^-_{m1} and ρ^-_{m1} in obvious notation.

To solve the discontinuity equations (B.21-B.23), we note that the component of the baryon current normal to the first discontinuity surface is

$$J_1 = \rho^-_{m1} \cosh(y^-_{m1} - \eta_{m1}) \ , \tag{C.3}$$

where

$$\eta_{mn} = \frac{1}{2} \ln \left(\frac{t_{mn} + z_{mn} - 2n\lambda/N_s}{t_{mn} - z_{mn}} \right) \tag{C.4}$$

is the pseudorapidity variable at the intersection of the m^{th} recoil trajectory with the n^{th} source hyperbola. The effective mass m_{m1}, density ρ^+_{m1}, and the flow rapidity y^+_{m1} right after the first discontinuity are then determined from the discontinuity equations.

Between the first and second source discontinuities, the fluid continues to accelerate in the external field as parameterized in Eqs.(2.2) in terms of an effective string tension, σ^*. However, since the effective mass has changed to m_{m1}, the proper time constant (2.4) that characterizes the recoil trajectory in Eq.(A.3) must be changed from τ^*_{m0} to $\tau^*_{m1} = m_{m1}/\sigma^*$. Similarly, the recoil time constant between the j^{th} and $(j+1)^{th}$ discontinuities is given by

$$\tau^*_{mj} = m_{mj}/\sigma^* \ . \tag{C.5}$$

Therefore, the m^{th} cell recoil trajectory between the j^{th} and $(j+1)^{th}$ discontinuities is given by

$$(z - z_{mj} + \tau^*_{mj} \cosh y^+_{mj})^2 - (t - t_{mj} + \tau^*_{mj} \sinh y^+_{mj})^2 = \left(\tau^*_{mj}\right)^2 \ . \tag{C.6}$$

Solving (C.1,C.6) with $n = j+1$ for (t, z) gives $(t_{m(j+1)}, z_{m(j+1)})$ for the intersection of tha m^{th} recoil trajectory with the $(j+1)^{th}$ hyperbola. Note that for Model I, $\tau^* = \infty$ and the trajectory (C.6) reduces to a straight line.

The recoil rapidity just before the $(j+1)^{th}$ discontinuity is according to (A.2)

$$y^-_{m(j+1)} = \cosh^{-1} \left((z_{m(j+1)} - z_{mj})/\tau^*_{mj} + \cosh y^+_{mj} \right) \ . \tag{C.7}$$

The change of the proper time of the fluid element between the discontinuities is thus

$$\Delta\tau_{mj} = \tau^*_{mj}(y^-_{m(j+1)} - y^+_{mj}) \ . \tag{C.8}$$

For Model I, $\Delta\tau = \Delta t/u^0$ and of course $y^-_{m(j+1)} = y^+_{mj}$.

The (de)compression factor resulting from the propagation between the j and $(j+1)^{th}$ discontinuity is estimated from eq.(B.36). In order to compute that factor we must first estimate the local rest frame rapidity gradient, y'_{mj}, immediately after jumping over the j^{th} source. At (t_{mj}, z_{mj}) just after the discontinuity, the flow

rapidity is y^+_{mj} and the density is ρ^+_{mj}. At that same time in the local rest frame, the $(m+1)^{th}$ element is located at the intersection of

$$z = z_{mj} + (t - t_{mj})/v_{mj} \ , \tag{C.9}$$

$$(z - z_{(m+1)j} + \tau^*_{(m+1)j} u^0_{(m+1)j})^2 - (t - t_{(m+1)j} + \tau^*_{(m+1)j} u^1_{(m+1)j})^2 = \left(\tau^*_{(m+1)j}\right)^2 \ . \tag{C.10}$$

Eq.(C.9) just specifies the hypersurface of equal time in the m^{th} element's local rest frame. The second equation defines the approximate trajectory of the $(m+1)^{th}$ fluid element. Denoting the solution of (C.9,C.10) by $(t'_{(m+1)j}, z'_{(m+1)j})$, the local rest frame separation of the m and $(m+1)^{th}$ cells at lab time t_{mj}, immediately after the j^{th} discontinuity, is

$$\Delta z^+_{mj} \approx (z'_{(m+1)j} - z_{mj})/u^0_{mj} \ . \tag{C.11}$$

The rapidity of the $(m+1)^{th}$ cell at time $t'_{(m+1)j}$ is $\tilde{y}_{(m+1)j}$, as obtained by evolving the $(m+1)^{th}$ cell with eq.(A.2):

$$\tilde{y}_{(m+1)j} = \cosh^{-1}\left((z'_{(m+1)j} - z_{(m+1)j})/\tau^*_{(m+1)j} + \cosh(y^+_{(m+1)j})\right) \ . \tag{C.12}$$

The local rest frame rapidity gradient is then approximated as

$$y'_{mj} \approx (\tilde{y}_{(m+1)j} - y^+_{mj})/\Delta z^+_{mj} \ . \tag{C.13}$$

In practice, we estimate this rapidity gradient to second order accuracy using two neighboring cells. Knowing the change in proper time (C.8) and the rapidity gradient we can now solve for the compression $\rho^-_{m(j+1)}$, immediately before the $(j+1)^{th}$ discontinuity, using eq.(B.36).

Using Eq.(2.10), we can also estimate the change in the effective mass in the source free region as

$$\frac{m^*(\tau + \Delta\tau)}{m^*(\tau)} = \left(\frac{\rho(\tau + \Delta\tau)}{\rho(\tau)}\right)^{c_0^2} \ . \tag{C.14}$$

Thereby, we can estimate the sensitivity of the results to variations of the equation of state.

Finally, with $\rho^-_{m(j+1)}$ so determined, $y^-_{m(j+1)}$ given by (C.7), and the intersection coordinates determined from solving (C.1,C.6) with $n = j+1$, we can now compute the normal baryon current, J_{j+1}, at the $(j+1)^{th}$ discontinuity from (C.3). The relevant quantities across the $(j+1)^{th}$ discontinuity are then computed using eqs.(B.21-B.23). This evolution from the j to the $(j+1)^{th}$ discontinuity is performed for all cells until they emerge from the source region. In Model II, the evolution of the k^{th} cell terminates after it has crossed the kN_s/N_c^{th} source discontinuity. Beyond that point it is assumed that the local external field has been neutralized and that cell would evolve according to the source free hydrodynamic equations.

These recursion relations are simple to implement numerically and solve via the Lagrangian method the hydrodynamic equations (2.6,2.7) for the special case of a dust equation of state. Using (C.14) the sensitivity to the equation of state can be estimated. A full solution for the case with $c_0 \neq 0$ would also require solution of (2.11).

Bibliography

[1] R. Anishetti, P. Koehler, and L. McLerran, Phys. Rev. D22, (1980) 2793.

[2] Proc. Bielefeld Workshop, Quark Matter Formation and Heavy Ion Collisions, eds. M. Jacob, H. Satz (World Scientific, Singapore, 1982);
Quark Matter '83, eds. T.W.Ludlam, H.E.Wegner, Nucl. Phys. A418 (1984) 1c; Quark Matter '84, ed. K. Kajantie, Lecture Notes in Physics 221 (Springer-Verlag, Berlin 1985).

[3] M. Gyulassy, Proc. Bielefeld Workshop, op. cit., p. 81.

[4] K. Kajantie, R. Raitio, and V. Ruuskanen, Nucl. Phys. B222 (1983) 152;
R. Raitio, Nucl. Phys. A418 (1984) 539c.

[5] R.C.Hwa, Nucl. Phys. A418 (1984) 559c.

[6] J.D.Bjorken, Phys.Rev. D27 (1983) 140.

[7] M. Gyulassy and T. Matsui, Phys. Rev. D29 (1984) 419.

[8] W. Busza, A. Goldhaber, Phys. Lett. 139B (1984) 235;
A. Barton, *et al.*, Phys. Rev. D27 (1983) 2580.

[9] L.P. Csernai, J. Kapusta, Phys.Rev. D29 (1984) 2664; D31 (1985) 2795.

[10] S. Date, M. Gyulassy, H. Sumiyoshi, Phys. Rev. D32 (1985) 619.

[11] R.J. Ledoux, et. al., Proc. of XIV Workshop on Gross Properties of Nuclei and Nuclear Excitations (Hirschegg, Austria) 1986, MIT-preprint.

[12] H. Ehtamo, J. Lindfors, L. McLerran, Zeit. Phys. C18 (1983) 341.

[13] T.S. Biro, H. B. Nielsen, and J. Knoll, Nucl.Phys. B245 (1984) 449.

[14] A. Bialas, W. Czyz, Phys. Rev. D31 (1985) 198.

[15] K.Kajantie and T.Matsui, Phys. Lett. 164B (1985) 373.

[16] A. K. Kerman, T. Matsui, B. Svetitsky, Phys. Rev. Lett. 56 (1986) 219.

[17] M. Gyulassy and A. Iwazaki, Phys. Lett. B165 (1986) 157.

[18] see review by N.N. Nikolaev, Sov. J. Part. Nucl. Phys. 12 (1981) 63.

[19] K. Kajantie, L. McLerran, Nucl. Phys. B214 (1983) 261.

[20] H.-Th. Elze, M. Gyulassy, D. Vasak, LBL-21137 preprint (1986), Nucl. Phys. B in press.

[21] A. Hosoya and K. Kajantie, Nucl. Phys. B250 (1985) 666.

[22] P. Danielewicz and M. Gyulassy, Phys. Rev. D31 (1985) 53.

[23] S. Gavin, Nucl. Phys. A435 (1985) 826.

[24] A.H. Taub, Phys. Rev. 74 (1948) 328.

[25] L.P. Csernai, Phys. Rev. D29 (1984) 1945.

[26] L.P. Csernai, Submitted to Sov. JETP.; L.P. Csernai and T. Matsui, LBL-18175(1984) and UMTNP-109/1984 preprints.

[27] C. DeMarzo, *et al.*, Phys. Rev. D29 (1985) 363.

[28] L.D. Landau and E.M. Lifsitz: Fluid dynamics (Pergamon, 1959)

[29] K.S. Thorne, Astrophys. J. 179 (1973) 897.

[30] E.V. Shuryak, Phys. Rep. 61 (1980) 71.

[31] M. Gyulassy, Nucl. Phys. A418 (1984) 59.

[32] L. McLerran, in Quark Matter '84, op. cit., p1.

Figure Captions:

1. Space-time picture of recoil and color neutralization. As a result of interactions between projectile and target at depths z_0 and z_1, two incoherent strings neutralize along hyperbolas indicated. The fluid cell initially at depth z_1 follows the dashed world line.

2. Evolution of a fluid cell initially three mean free paths deep in the target ($z_0 \approx$ 6.9 fm) as a function of its proper time. Dashed (solid) curves correspond to Model I (Model II). Solid curves are labeled by the projectile thickness in mean free paths, ν_P. For Model I $\nu_P = 6$ is assumed. Part (a) shows the characteristic difference between the two models. The four velocity divergence is positive for Model I but negative for Model II. The evolution of the energy density in that cell is shown in part (b). The curves terminate at the proper time when the cell emerges from the source region.

3. The maximum energy and baryon densities reached at the time when fluid cells emerge from the source region as a function of their initial depth in the target. Parts (a) and (c) correspond to Model II. Parts (b) and (d) correspond to Model I. The projectile thickness is indicated by the number of mean free paths ν_P. The dashed curves test the sensitivity to changes in the equation of state ($c_0^2 = 0 - 1/3$) for the case $\nu_P = 6$. See section 3.2 for details.

4. The flow rapidities of cells as they emerge from the source region. Parts (a,b) refer to Models II and I respectively. Notation is same as in Fig.4.

5. Proper time development of recoil rapidity (a), baryon density (b), and enthalpy (c). Solid curves correspond to dust equation of state. Short and long dashed lines correspond to $p = c_0^2(\epsilon - \epsilon_0)$ with $c_0^2 = 1/6, 1/3$ respectively.

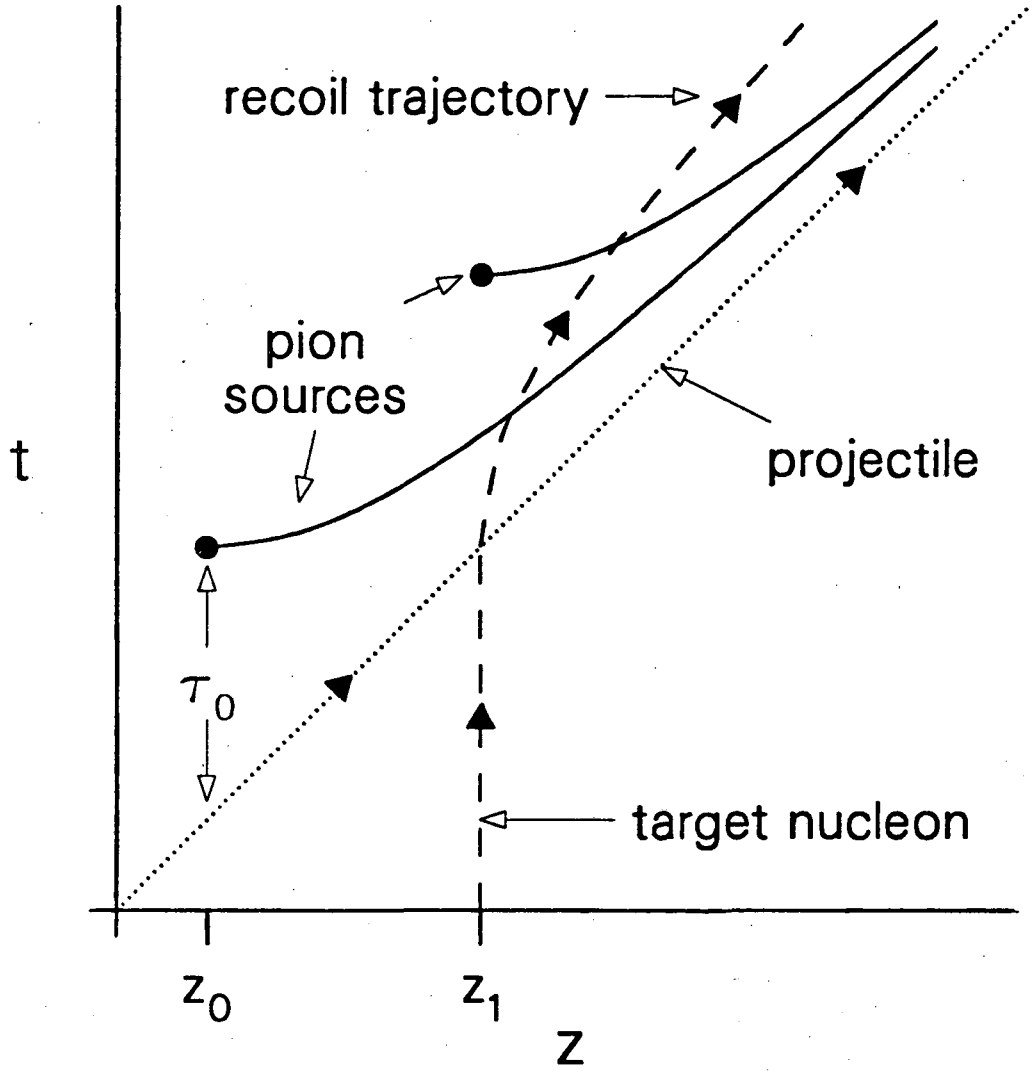

XBL 865-2016

Fig. 1

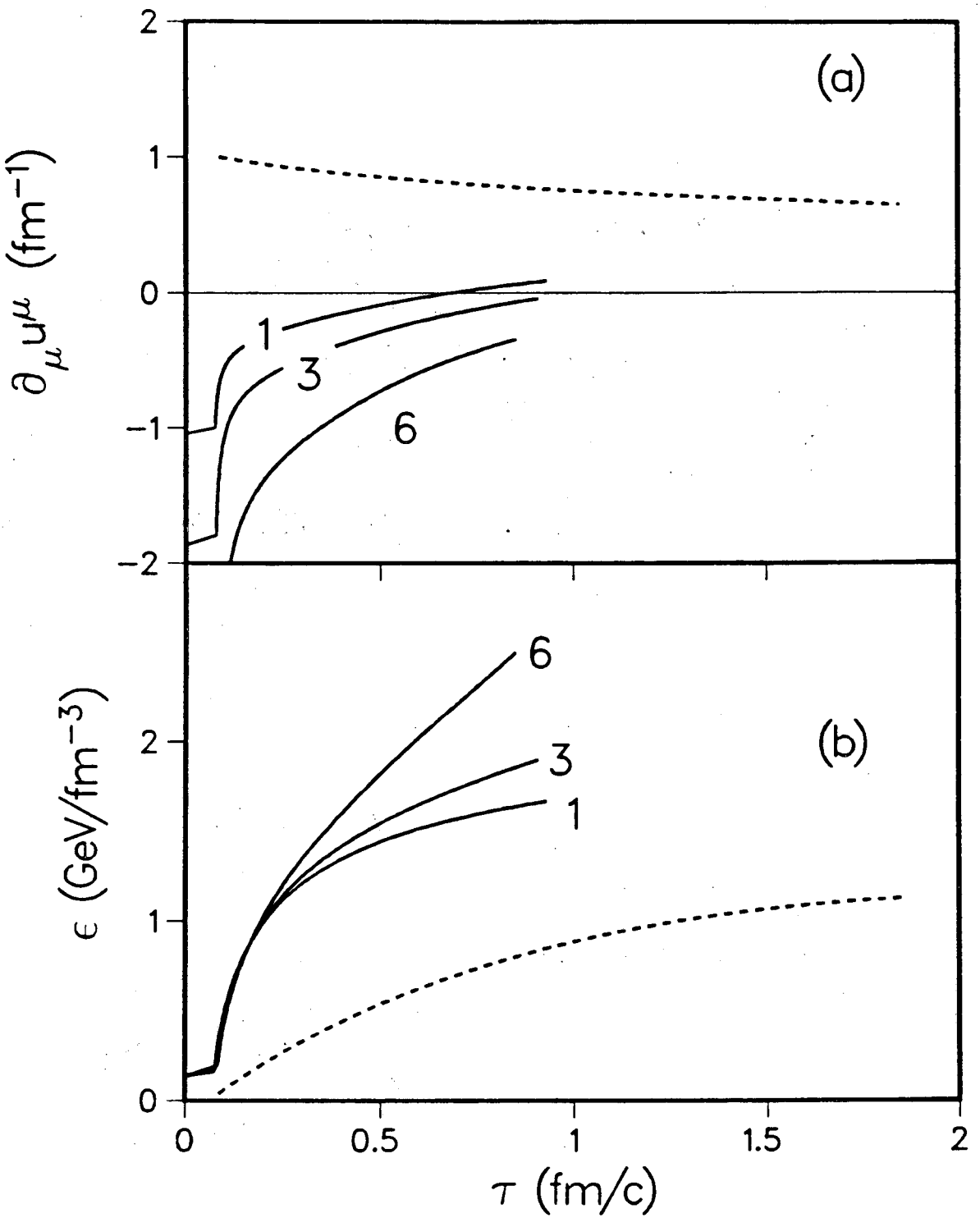

XBL 865-2018

Fig. 2

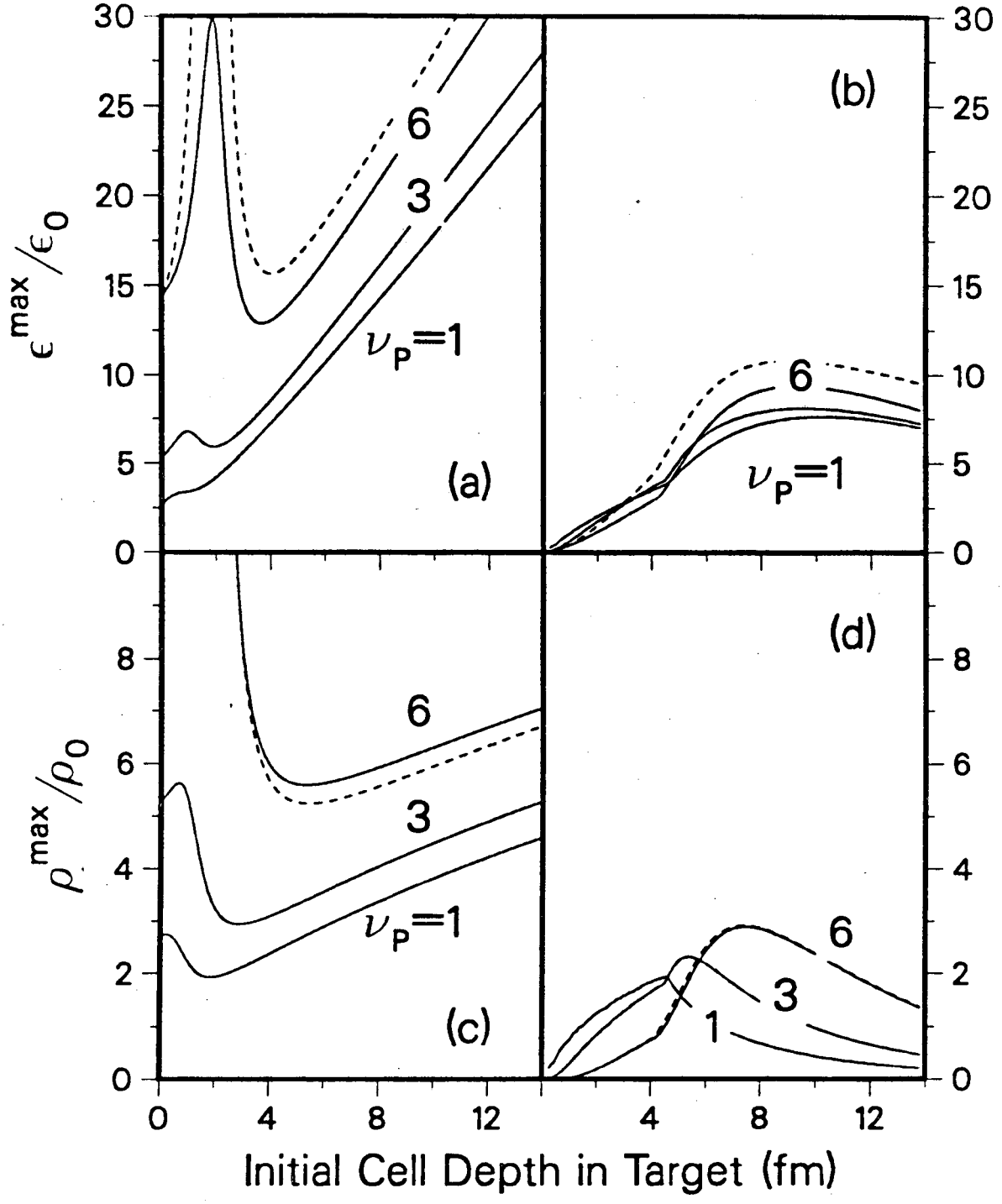

XBL 865-2017

Fig. 3

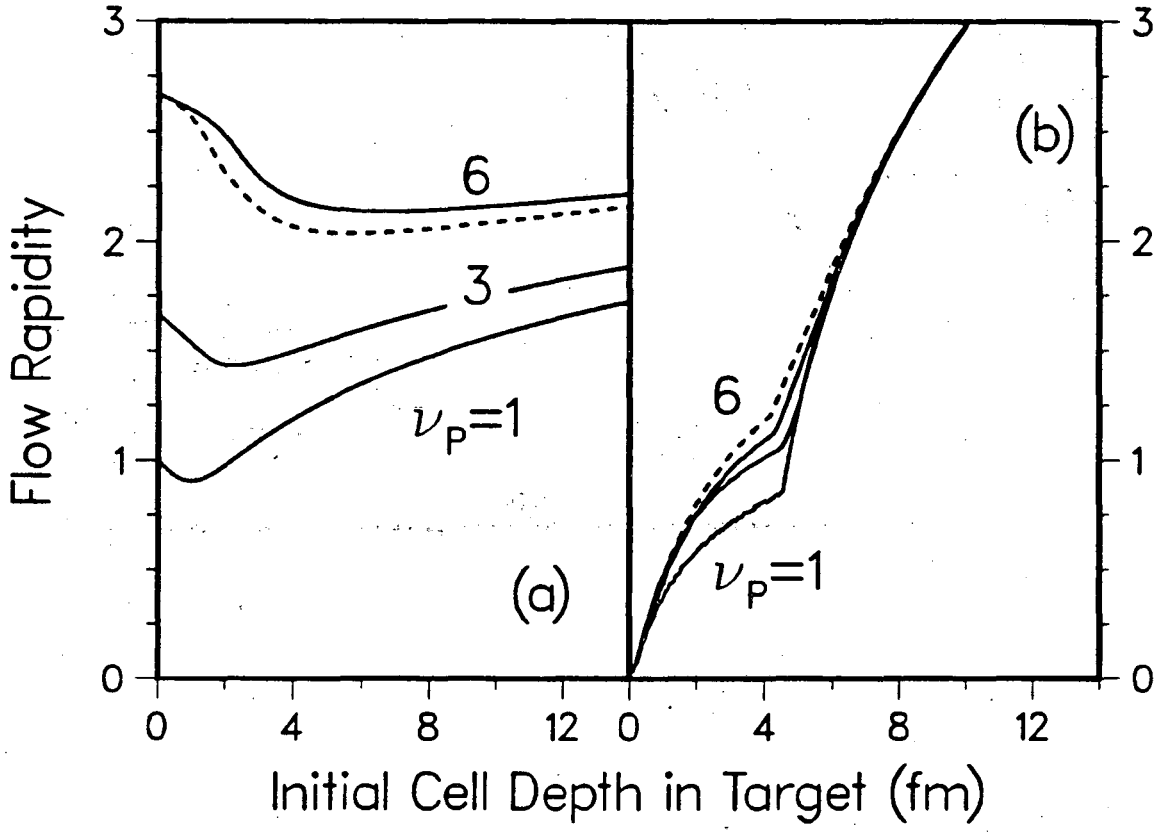

XBL 865-2015

Fig. 4

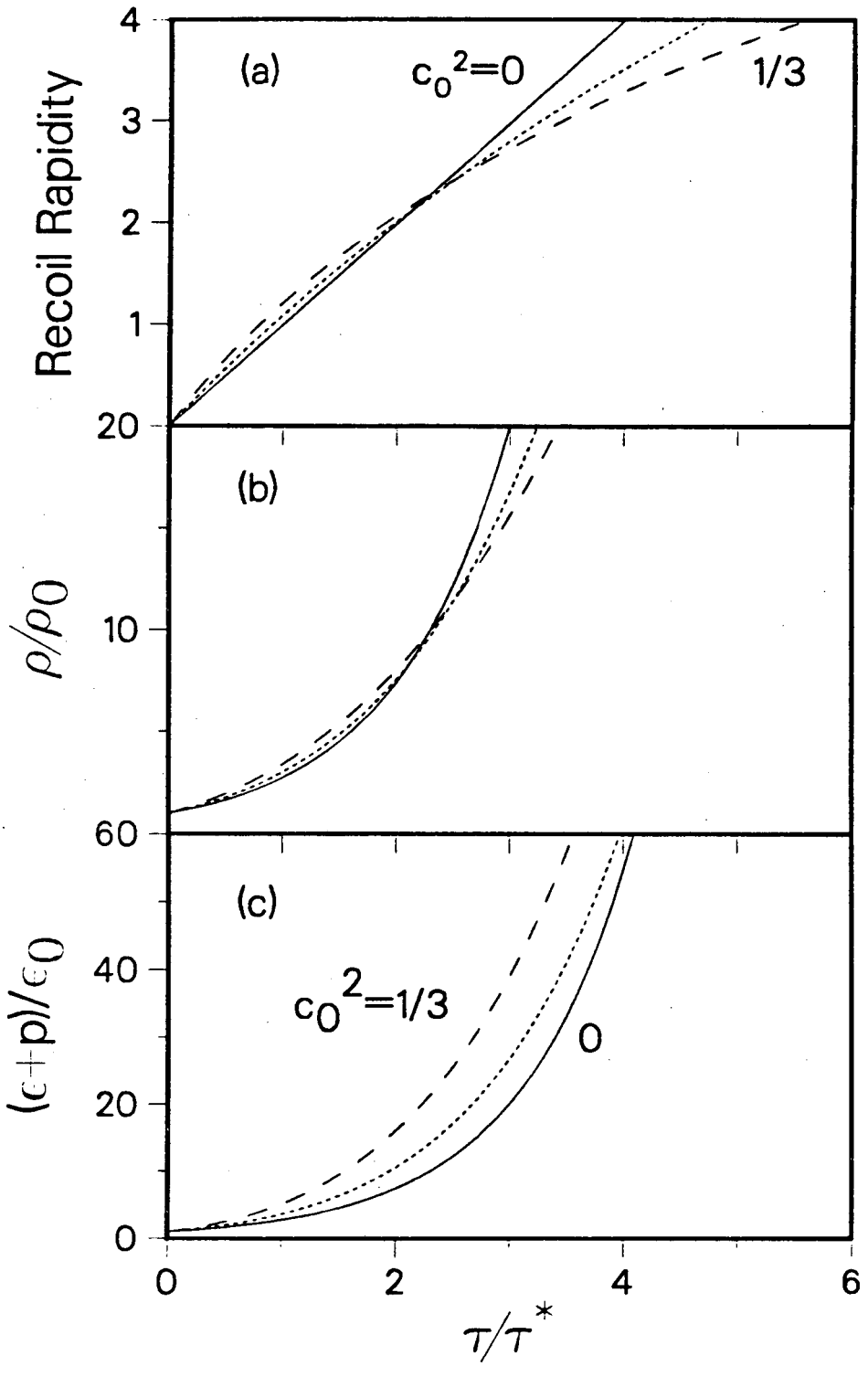

XBL 865-2019

Fig. 5

LAWRENCE BERKELEY LABORATORY
TECHNICAL INFORMATION DEPARTMENT
UNIVERSITY OF CALIFORNIA
BERKELEY, CALIFORNIA 94720